Utrecht University

MASTER THESIS

Engineering of impurity bands with Chern Numbers

Author:
Emma MINARELLI

Supervisor:
Lars FRITZ

A thesis submitted in fulfillment of the requirements
for the degree of Master Thesis
in the
Graduate School of Natural Science
Institute of Theoretical Physics

August 13, 2018

Universiteit Utrecht

to my mother Antonella,
to my father Enzo

Abstract

Recently, there have been studies on p-wave superconductor system designed with a lattice of impurity over its surface. They result in non-trivial topological phases with high-values of Chern Numbers.
The present thesis investigates a similar model starting with a 3D strong Topological Insulator - experimentally established. Focusing on one surface, first we place a ferromagnetic material to create an energy gap on the surface spectrum, then we display a square rarefied lattice of magnetic impurities. That is a two-bands model and we derive for it an effective Hamiltonian. Calculating the Chern Numbers of the in-gap bands structure and studying the surface energy spectrum, we find the setting responds like a Chern Insulator.
Finally, comparing the spectrum energy initial condition of our model to the p-wave superconductor one, we mention the next improvements to eventually reach high-values of Chern Numbers.

Acknowledgements

This thesis is the outcome of a great journey. And some people have played an essential role in it.
First of all, my advisor Lars Fritz. Thanks for developing such interesting discussions around the project - enforcing the physical intuition behind each issue, for answering all my questions and showing me your critical approach to treat problems. Thanks for giving me further motivation and insights when you saw I needed. And thanks for always accepting all my last-minute-requests of meeting.
Secondly, the PhD student Gerwin van Dalum. Thanks for giving me your help any time I needed. Thanks for the critical analyses and the discussions about any possible issues, adding any further comments to improve my work. Indeed, I have learnt a lot from you.
Then, the prof. Cristiane Morais Smith. Thanks for sharing your passion and enthusiasm in physics. Thanks for being such a trustable person.
Then, I had the pleasure to travel these years with some amazing fellow students. Domingo - I have learnt so much from your deep knowledge and now, even at distance, I know I have such a good friend like you; Enea - discussing about many topics with a wise and smart person like you, it has been a true gift; Charlotte - even though you reached us almost at the end, it seems we know each other since ages and that is surprising; Peter - for our unforgettable discussions about my project, I will definitely miss talking about physics with you; Folkert, for being such a genuine combination of a hardworking/reliable/friendly person; Adriana, the most joyful of all of us because we do need joy in life; Patrick - such a sensitive person; Kevin - for trying to make me use the Dubliner's accent, so happy to have a friend like you in Dublin already.

This journey has a complementary side, an artistic one. Among the many workshops, performances and people I have experienced in Amsterdam, thanks to the performer Katie D. for teaching me how to flow-pause-exit not only on stage but in daily life too.

Many people have contributed to make me feel at ease in Utrecht, many others to make me feel as if I were still at home in Italy. Among all of them I cannot deny an official mention to:
Rebecca - we have been (and hopefully we will be) always such precious friends, wherever we are;
Federica - sharing pieces of life and experience since (more than) 7 years ago;
Alice - a powerful, brilliant woman, such a blessing we have met;
Chiara - as if you were my elder sister, and much more.

However, my biggest gratitude goes to my parents. Thanks for always being with me - even though at distance, always believing in me, supporting my choices and giving me any help when I needed. Thanks for accepting that your only daughter is running all over Europe, from Berlin to Utrecht and now to Dublin. And thanks for providing me a solid culture and a deep artistic education, which perfectly completes my academic background.

Contents

Chapter 1

The Prolegomena to the Model

1.1 Models for band structure and gap energy formation

We start with a review of processes to create band structure - associated to a dispersive energy spectrum - and gap energy - a forbidden energy range in the system. We discuss two complementary approaches, namely the **nearly free electron model** and the **tight-binding model**. In due course, we introduce some basic concepts of solid-state physics.
Further reading can be found in Atland and Simons [1], Bruus and Flensberg [2], Parker [3], Sigrist [4].

1.1.1 Models with potential

A simple model to describe electrons is a system without interactions and with negligible potential, i.e. $V(\mathbf{r}) = V_0$ constant. It is defined as **free electron model**: its Schrödinger wave equation is solved by plane wave solutions and its energy dispersion is quadratic.
More realistic models consider delocalised free electrons under the influence of a periodic potential, i.e. an additional weak periodic potential is switched on: $V(\mathbf{r}+\mathbf{R}) = V(\mathbf{r})$ with $\mathbf{R} = a\mathbf{e}_i$ and a lattice constant. They are defined as **nearly free electron model**: Bloch waves are used as wave equation solution and the dispersion assumes a non-quadratic trend with a characteristic bands and gaps.

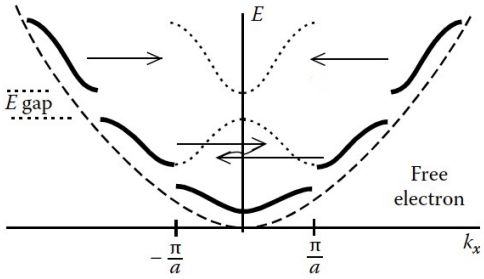

Figure 1.1: In 1D system, comparison between the energy dispersion between free electrons (dashed curve) and nearly free electrons either within the first *Brillouin zone* (FBZ) i.e. $k \in [-\pi/a, \pi/a]$ (dotted curves) or shifted outside the FBZ (solid curves) using reciprocal lattice. Note the opening of energy band gap for the latter model. [3]

The presence of a periodic potential creates *band structures* in the system, meaning the energy spectrum $E = E(\mathbf{k})$ divides into two areas, see figure above. They are referred to some energy values belonging to the allowed sectors, where the density of states $\rho(E)$ is non-zero. Some others are inside the forbidden areas, where no states can be found: $\rho(E) = 0$: that leads to the separation of bands by a *gap*. The boundary between band and gap is denoted by *band edge*.

1.1.2 Tight-Binding Model

We consider a system with N atoms arranged on a lattice. Each atom has got the same discrete non-degenerate energy levels and a local interaction potential. Hence, at each site the potential is similar to the attractive-like Coulomb potential (see fig.1.2a).
Furthermore, we consider a rarefied lattice. In such a case, the distance among neighboring atoms admits only a slight overlap of their outer electron wave functions. Under this condition, known as **Tight-Binding** limit, the electronic wave function of lower energy levels is mostly *localized* at the atomic core, since these electrons are protected by outer electrons. Higher energy levels, due to the least strength of binding energy, can spread and delocalise on neighboring atomic sites. Each energy level will split into N sub-levels to form a band structure, which is defined by a corresponding band index n. Thus, due to these itinerant electrons the original discrete levels of the energy spectrum disperses (see fig.1.2b) and a gap in such structure may arise. The process of electrons jumping from one site to an other is called *hopping process*.

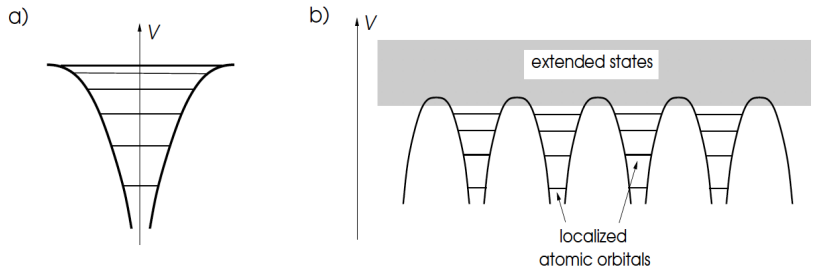

Figure 1.2: (a) An isolate atom satisfies the single-particle Hamiltonian and its energy spectrum has discrete levels. (b) A lattice under tight-binding condition. The lower energy levels belong to the atomic core; the higher energy levels are allowed to overlap with the neighbor levels. These states are responsible for both splitting energy levels and occurring band structures. [4]

We have seen so far the two complementary strategies to create band structure. On one side, the nearly free electrons model is a system of delocalised free atoms which needs an external periodic potential to make dispersive the energy spectrum. On the other side, the Tight-Binding Model considers localised atom systems with a local energy and potential where we allow hopping processes, resulting in bands.
Going back to Tight-Binding Model, we discuss some property of it. The Hamiltonian of the system is $\hat{H} = \hat{H}_0 + V(\mathbf{r})$, where the first term contains the local energy ϵ_0.
First, we discuss about the effect of local periodic potential of each atom: it makes the Hamiltonian $\hat{H}$ invariant under discrete lattice translations. Introducing the translation operator $\hat{T}_a$, we note it commutes with the Hamiltonian:

$$[\hat{H}, \hat{T}_a] = 0.$$

It means there exists a complete set of eigenfunctions that simultaneously are eigenstates of $\hat{H}$ and $\hat{T}_a$. This set is given by **Bloch functions**, product of plane wave solution and a periodic function $u_{n,\mathbf{k}}(\mathbf{r} + a\mathbf{e}_i) = u_{n,\mathbf{k}}(\mathbf{r})$ on each unit cell $[0, a]$ of the lattice - note it has the same periodicity as the potential $V(\mathbf{r})$:

$$\psi_{n,\mathbf{k}}(\mathbf{r}) = \frac{1}{\sqrt{V}} e^{i\mathbf{k}\cdot\mathbf{r}} u_{n,\mathbf{k}}(\mathbf{r})$$

where $\mathbf{k}$ is defined in FBZ and n is an integer quantum number called *energy band index* which labels the complete set of $u_{n,\mathbf{k}}(\mathbf{r})$.
Hence, the final expression of the Schrödinger wave equation for nearly free electrons model reads:

$$\hat{H}\psi_{n,\mathbf{k}}(\mathbf{r}) = E_n(\mathbf{k})\psi_{n,\mathbf{k}}(\mathbf{r}),$$

it is given in terms of Bloch functions and a dispersive energy spectrum. This representation choice of wave functions is called **Bloch Theorem**.
Then, we regard the overlapped-wave functions: they belong only to the nearest neighboring lattice site. In order to calculate, approximately, the global overlapped-wave function of the system we can use the *linear combination of atomic orbitals* (LCAO):

$$\tilde{\psi}_{n,\mathbf{k}}(\mathbf{r}) = \frac{1}{\sqrt{N}} \sum_{\mathbf{r}_i} e^{i\mathbf{k}\cdot\mathbf{r}_i} \psi_{n,\mathbf{k}}(\mathbf{r})$$

where $\mathbf{r}_i$ with $i = 1, ..., N$ indicates positions over the lattice and $\psi_{n,\mathbf{k}}(\mathbf{r})$ is the Bloch wave function.
We already pointed out the system is localised: we need a proper solution to solve the Schrödinger equation for a Tight-Binding Model. Instead of solving it using Bloch wave function $\psi_{n,\mathbf{k}}(\mathbf{r})$ - they delocalise across the lattice - we introduce localised atomic states, called *Wannier function* $W_n(\mathbf{r} - \mathbf{R})$. They are centered at the lattice site $\mathbf{R} \equiv \mathbf{r}_i$ and they are defined as the Fourier Transform of the Bloch wave function, namely:

$$W_n(\mathbf{r} - \mathbf{R}) = \frac{1}{\sqrt{N}} \sum_{\mathbf{k}}^{FBZ} e^{-i\mathbf{k}\cdot\mathbf{R}} \psi_{n,\mathbf{k}}(\mathbf{r})$$

and they obey orthogonality relation:

$$\int d^3r W_n^*(\mathbf{r} - \mathbf{R}') W_n(\mathbf{r} - \mathbf{R}) = \delta_{\mathbf{R}'\mathbf{R}}.$$

The Wannier function can be used to express the band energy $\epsilon_{\mathbf{k}}$ of the system:

$$\begin{aligned}
\epsilon_{\mathbf{k}} &= \epsilon_0 + \sum_{\mathbf{R}} t(\mathbf{R}) e^{-i\mathbf{k}\cdot\mathbf{R}} \\
\epsilon_0 &= \int d^3r W_n^*(\mathbf{r}) W_n(\mathbf{r}) \\
t(\mathbf{R}) &= \int d^3r W_n^*(\mathbf{r} - \mathbf{R}') H W_n(\mathbf{r})
\end{aligned}$$

where $t(\mathbf{R})$ represents the strength of the hopping process in $\mathbf{r}$-space and ϵ_0 represents the energy band of a system with no interatomic coupling - hence the local energy. Thus, only in case of overlapped atomic orbitals, the hopping process will assume a relevant role in the formation of band structures.

For the following purposes, we introduce the **second-quantized Hamiltonian** regarding a system of electronic bands in Tight-Binding approximation. Without loss of generality, we assume spinless electrons, single-orbital band $n = 1$ in a 1D lattice with periodic boundary condition.
We introduce fermionic operators i.e. $c_i^\dagger, c_i$ which creates and annihilates an electron on lattice site $\mathbf{r}_i$ respectively.
In real space, the Hamiltonian for N number of lattice sites reads:

$$H = \sum_i \epsilon_0 c_i^\dagger c_i - \sum_{ij} t_{ij} c_i^\dagger c_j, \tag{1.1}$$

where ϵ_0 is the single-particle energy and t_{ij} is the matrix element strength of the hopping process among electrons. Currently, we assume the summations are running over all lattice sites.
Using the Fourier Transform, we go to momentum space:

$$c_i^\dagger = \frac{1}{\sqrt{N}} \sum_k^{FBZ} a_k^\dagger e^{-ik(ar_i)}$$

with a lattice constant of the system and $k = (2\pi/aN)n, \quad n \in [0, N]$.
Finally, we can perform the transformation:

$$H_k = \sum_k \Big(\epsilon_0 - \overbrace{\frac{1}{N}\sum_{ij} t_{ij} e^{-ika(r_i - r_j)}}^{t_k}\Big) a_k^\dagger a_k$$
$$\Rightarrow \boxed{H_k = \sum_k \epsilon_k a_k^\dagger a_k} \tag{1.2}$$

and that results into the second quantized Hamiltonian in momentum space with ϵ_k the *energy dispersion*.

1.1.3 Metals and Insulators

The Bloch functions $\psi_{n,\mathbf{k}}(\mathbf{r})$ have been introduced to describe electrons in systems which are controlled by periodic potential. The study of corresponding energy spectrum $E = E_n(\mathbf{k})$ offers an explanation to different band configurations.
We define the highest occupied band as **valence band** and the lowest empty band as **conductance band**. In agreement with the Pauli Exclusion Principle, we can fill electrons in the system starting from the lowest level, the ground state, and double occupancy of the same state is forbidden.

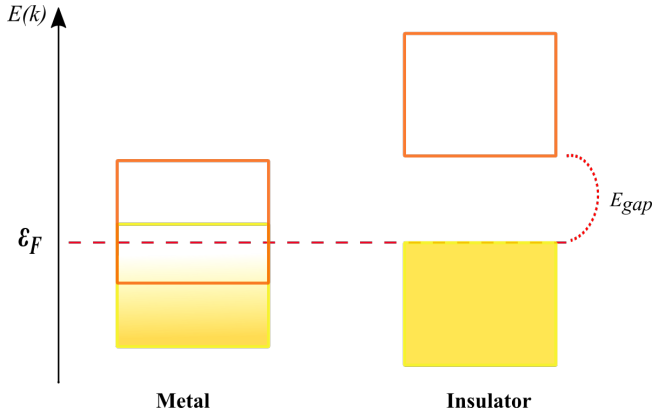

Figure 1.3: Scheme of energy bands for a metal and an insulator (or semiconductor). The former has overlapped bands with a partially filled valence band. The latter has energy gap with a completely-filled valence band.

Partially-filled bands will be achieved if only part of the allowed states are occupied. *Completely-filled bands* are identified if the number of accessible electrons in the system occupies all the states, resulting in a non-degenerate state. In the former case, we refer to the highest occupied energy level (with 50% probability of occupation) to *Fermi Level* ϵ_F. It corresponds to the chemical potential at zero temperature: $\lim_{T\to 0} \mu(T) = \epsilon_F$. It follows the properties of a systems with multiple bands are given by only the valence and conductance bands, since they are the closest to ϵ_F.
According to the position of the Fermi Level in the spectrum, see figures above and below, we consider two classes:

- **Metals**: the valence band is partially filled and the ϵ_F level lies inside it. There is no energy gap that makes a distinction between valence and conductance band: the two bands indeed overlap. Any small perturbation applied (provided by external field or radiation, heat source), the system responds modifying the occupation particle state. Indeed, metals conduct thermal energy and electric current.

- **Insulators**: the valence band is completely filled and the ϵ_F level coincides with its maximum energy level. There is an energy gap E_{gap} between valence and conductance band. Hence, energy excitation comparable to the energy gap are required to alter the occupation level. This explains the lack of heat and electric transport for small perturbations, since any $E < E_{gap}$ will not change the particle state in insulators.

In particular, at zero temperature, insulators with small energy gap $E_{gap} \lesssim 2eV$ are called *semicondutors*: at room temperature they can significative conduct electricity, meaning they display intermediate properties between insulators and metals.

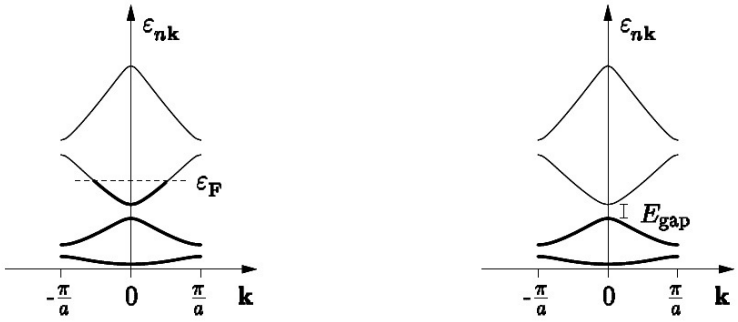

Figure 1.4: On the left band structure of a metal: the presence of Fermi Level inside the bands makes metals highly reactive to small perturbations. On the right band structure of insulator/semiconductor: since the Fermi Level is equal to the highest level of the valence, small perturbation will not affect the particle occupation. Band structures are defined within FBZ. [2]

1.2 Impurity scattering

Every deviation from a regular array of atoms is source of defect or impurity scattering.
The definition of the **impurity problem** we are going to study is the following, as schematically pictured below.

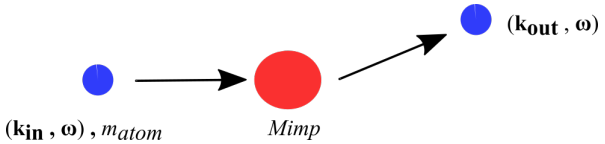

Figure 1.5: Sketch of the impurity problem.

We consider a periodic lattice of atoms broken by the presence of one impurity, neither charged nor magnetic.
The impurity is **static** - meaning the impurity mass is much bigger than one of the other atoms i.e. $\frac{M_{imp}}{m_{atom}} \gg 0$. It follows the presence of impurity doesn't contribute to variation in energy, only to change propagation direction of the scattered particle i.e. $\mathbf{k}_{in} = |k|e^{i\theta_{in}}$ is different from $\mathbf{k}_{out} = |k|e^{i\theta_{out}}$ for isotropic dispersion.
The impurity is **structureless** - it only has got translational degree of freedom. Hence, it exchanges only linear momentum and the resulting scattering process is **elastic**, since energy is conserved but transfer of momentum happens.
Moreover, the presence of the impurity determines a lack of translational invariant in the system: after the scattering the original momentum of the incoming particle is lost.

In a collection of impurity on a lattice, averaging over all possible paths taken by the scattered particle is the method to make the system again diagonal in momentum space.

In this section we are going to study a different approach which doesn't require the averaging of impurity configuration. Then, we calculate the conditions to find *bound states* in the system.
Further reading can be found in Economou [5], Mahan [6] and Atland and Simons [1].

1.2.1 Integral equation for Schrödinger wave equation

We introduce how to solve the Schrödinger equation using **Green's function method** before the actual study of scattering processes.
Starting from $|\mathbf{r}\rangle$ basis eigenvector of position operator, we define the wave function of an arbitrary eigenstate $|\psi_n\rangle$ in such a representation:

$$\psi_n(\mathbf{r},t) = \langle \mathbf{r}|\psi_n(t)\rangle$$

where n index means the values taken by the eigenfunctions. This is an orthonormal function whose set is complete, namely:

$$\langle \mathbf{r}|\mathbf{r}'\rangle = \delta(\mathbf{r}-\mathbf{r}') \quad , \quad \int d\mathbf{r}\, |\mathbf{r}\rangle \langle \mathbf{r}| = 1.$$

The **time-dependent Schrödinger equation** reads:

$$\hat{H}(\mathbf{r},t)\psi_n(\mathbf{r},t) = E_n\psi_n(\mathbf{r},t) \quad \Rightarrow \quad (E_n - \hat{H}(\mathbf{r},t))\psi_n(\mathbf{r},t) = 0 \tag{1.3}$$

where E_n is the eigenvalue for the eigenstate $|\psi_n\rangle$ of the operator $\hat{H} = \hat{H}_0 + V^{ext}$, with $\hat{H}_0$ free particle Hamiltonian and V^{ext} generic external potential.
The corresponding **Green's function** to the Schrödinger equation satisfies:

$$\big(i\partial_t - \hat{H}(\mathbf{r},t)\big)G(\mathbf{r},\mathbf{r}';t,t') = \delta(\mathbf{r}-\mathbf{r}')\delta(t-t').$$

If we express the time-dependent Green's function in terms of its Fourier Transform, namely:

$$G(\mathbf{r},\mathbf{r}';t,t') = \int \frac{d\omega}{2\pi} e^{-i\omega(t-t')} G(\mathbf{r},\mathbf{r}';\omega).$$

Plugging this into the previous equation we derive a time-independent equation:

$$(\omega - \hat{H}(\mathbf{r}))G(\mathbf{r},\mathbf{r}';\omega) = \delta(\mathbf{r}-\mathbf{r}'). \tag{1.4}$$

Next, we want to find an expression for $G(\omega)$. The Hamiltonian is a Hermitian operator thus all its eigenvalues are real. In the complex plane, $G(\omega)$ is going to be an analytic function in all the plane with exception of those points or part of the real axis that correspond to the eigenvalues of $\hat{H}$. It will be clear that the simple poles (on the real axis) of the Green's function are located at the position of the discrete eigenvalues of the Hamiltonian and the inverse is valid too.
Now, we derive two expressions for $G(\omega)$ according to ω belongs or not to the energy spectrum of $\hat{H}$:

- ω is not an eigenvalue of $\hat{H}$, hence using the completeness of $|\mathbf{r}\rangle$ we can formally invert eq.(1.4):
$$G(\mathbf{r},\mathbf{r}';\omega) = (\omega - \hat{H}(\mathbf{r}))^{-1} \sum_n \psi_n^*(\mathbf{r}')\psi_n(\mathbf{r}) = \sum_n \frac{\psi_n^*(\mathbf{r}')\psi_n(\mathbf{r})}{\omega - E_n}$$
- in the relevant physical case, ω is an eigenvalue of $\hat{H}$ hence there exists a zero eigenvalue: the inverse of $\hat{H}$ is not defined in eq.(1.4). In order to avoid this issue, in the complex plane we need to remove the pole of $G(\omega)$ from the real axis by adding a positive infinitesimal quantity η so that the contour can still be evaluated on the real axis without poles. This procedure, called *analitycal continuation*, can be chosen for η going either from above or below to zero, leading to different planes of convergency.

The relative Green's functions are thus known as $G^+(\omega)$ **retarded propagator** and $G^-(\omega)$ **advanced propagator**. Hence, now that the singularity is removed from the path, $G^{\pm}(\omega^{\pm})$ is analytic again and gives the expression:

$$G^{\pm}(\omega^{\pm}) = \lim_{\eta \to 0^+} G(\omega \pm i\eta) = \lim_{\eta \to 0^+} \left((\omega \pm i\eta) - \hat{H}\right)^{-1} \tag{1.5}$$

We have all the elements of an implement to the study of wave equation. Instead of solving directly the differential equation of second order eq.(1.3), now that we have a criteria to derive the Green's function of the system, we can introduce the **integral wave equation** as solution of eq.(1.3):

$$\psi_n(\mathbf{r}) = \begin{cases} \int d^3\mathbf{r}' G_0(\mathbf{r}, \mathbf{r}'; \omega) V(\mathbf{r}') \psi_n(\mathbf{r}') & \text{for } \omega \neq E_n \\ \phi_n(\mathbf{r}) + \int d^3\mathbf{r}' G_0^{\pm}(\mathbf{r}, \mathbf{r}'; \omega) V(\mathbf{r}') \psi_n(\mathbf{r}') & \text{for } \omega = E_n \end{cases} \tag{1.6}$$

where the latter form is known also as *Lippman-Schwinger equation*. Note that $G_0(\omega)$ denotes the Green's function calculated from the free particle Hamiltonian $\hat{H}_0$.
Plugging the integral equation (1.6) into the Schrödinger equation (1.3) one can easily verify that is the actual solution:

$$\Big(E_n - \hat{H}(\mathbf{r})\Big)\psi_n(\mathbf{r}) = 0 \Rightarrow \begin{cases} \Big(E_n - \hat{H}_0(\mathbf{r})\Big)\phi_n(\mathbf{r}) = 0 \\ \Big(E_n - \hat{H}_0(\mathbf{r})\Big)\psi_n(\mathbf{r}) = V\psi_n(\mathbf{r}) \end{cases}$$

where $\phi_n(\mathbf{r})$ is the homogeneous solution. In case of **scattering states**, leading to a continuous energy spectrum, the Schrödinger equation has a particular solution $\phi_n(\mathbf{r})$; whereas for **bound states**, resulting into a discrete spectrum, there is none.
As final remark, starting from the knowledge of the Green's function, not only we have access to the energy spectrum of the system, hence to its eigenfunctions; we obtain also an alternative method to solve Schrödinger equation that will become quite useful in the following.

1.2.2 Hamiltonian of the scattering process

We start considering, without loss of generality, a 1D spinless electrons system in a regular lattice with one static non-magnetic impurity at its origin, as sketched in fig.(1.5).
In the first quantisation, its time-independent Hamiltonian can be identified by:

$$\hat{H}(\mathbf{r}) = \hat{H}_0(\mathbf{r}) + \hat{H}_{imp}(\mathbf{r}) = -\frac{\hbar^2}{2m}\nabla_{\mathbf{r}} + \sum_{i=1}^{N_{imp}} V_i.$$

where the first term stands for the free-particle Hamiltonian and the second term indicates the presence of an **impurity potential** - it is usually represented by a $\delta-$Dirac potential. In **r**-representation it reads

$$\hat{H}_{imp} = \sum_{i=1}^{N_{imp}} V_i = V_0 \sum_{i=1}^{N_{imp}} \delta(\mathbf{r} - \mathbf{R}_i),$$

where V_0 is the impurity strength (either repulsive or attractive for positive or negative values respectively).
Now, we switch to the second quantisation - a better frame to study the momentum dependence. We consider spinless electrons in a cubic box of size $V = L^3$ and we take periodic boundary conditions. Thus, the wave vector is: $\mathbf{k} = \frac{2\pi}{L}\mathbf{n}$, with $\mathbf{n} = (n_x, ny, n_z) \in \mathbb{Z}^3$.

We introduce creation and annihilation operators $c^\dagger_{\mathbf{k}}, c_{\mathbf{k}}$. The field operators are given by the Fourier Transform:

$$\psi(\mathbf{r})^\dagger = \frac{1}{\sqrt{V}}\sum_{\mathbf{k}}^{FBZ} c^\dagger_{\mathbf{k}} e^{-i\mathbf{r}\cdot\mathbf{k}}$$
$$\psi(\mathbf{r}) = \frac{1}{\sqrt{V}}\sum_{\mathbf{k}}^{FBZ} c_{\mathbf{k}} e^{i\mathbf{r}\cdot\mathbf{k}}$$

And the anti-commutation relations for fermions:

$$\{\psi(\mathbf{r}), \psi(\mathbf{r}')^\dagger\} = \delta(\mathbf{r}-\mathbf{r}')$$
$$\{\psi(\mathbf{r}), \psi(\mathbf{r}')\} = \{\psi(\mathbf{r})^\dagger, \psi(\mathbf{r}')^\dagger\} = 0$$

Hence, in the second quantisation, the impurity Hamiltonian then reads:

$$\hat{H}_{imp} = \int d\mathbf{r}\Big(V_0\sum_{i=1}^{N_{imp}}\delta(\mathbf{r}-\mathbf{R}_i)\Big)\psi^\dagger(\mathbf{r})\psi(\mathbf{r}) = \frac{V_0}{V}\sum_{i=1}^{N_{imp}}\sum_{\mathbf{k}\mathbf{k}'} c^\dagger_{\mathbf{k}'}c_{\mathbf{k}}e^{i\mathbf{R}_i\cdot(\mathbf{k}-\mathbf{k}')},$$

we note the outcome is not diagonal in **k**-representation. This is a further evidence of the absence of translationally invariant in the system once the impurity is set on the lattice. On the other side, the non-interacting part will still be diagonal in momentum space. Therefore, the final structure of the Hamiltonian in **k**-representation is given by:

$$\hat{H}_{\mathbf{k}} = \hat{H}_0(\mathbf{k}) + \hat{H}_{imp}(\mathbf{k}) = \frac{1}{V}\sum_{\mathbf{k}} c^\dagger_{\mathbf{k}}\epsilon_{\mathbf{k}}c_{\mathbf{k}} + \frac{|V_0|}{V}\sum_{\mathbf{k}\mathbf{k}'} c^\dagger_{\mathbf{k}'}c_{\mathbf{k}}$$

where $\epsilon_{\mathbf{k}}$ is the single-particle dispersion.
Next, going back to **r**-representation, we introduce the time-independent Schrödinger equation, see in analogy eq.(1.3):

$$(E - \hat{H}_0(\mathbf{r}))\psi(\mathbf{r}) = \hat{H}_{imp}\psi(\mathbf{r})$$

and its corresponding retarded Green's functions (see the discussion for eq.(1.5)) satisfy:

$$\Big(\omega^+ - \hat{H}(\mathbf{r})\Big)G^+(\mathbf{r},\mathbf{r}';\omega^+) = \delta(\mathbf{r}-\mathbf{r}')$$
$$\Big(\omega^+ - \hat{H}_0(\mathbf{r})\Big)G_0^+(\mathbf{r},\mathbf{r}';\omega^+) = \delta(\mathbf{r}-\mathbf{r}').$$

As previously seen, we have to determine a form of $G_0^+(\omega)$ in terms of $\hat{H}_0$. Taking the already calculated eq.(1.5) and recalling that the non-perturbed part describes a translationally invariant system, i.e. $\nexists V^{ext}$, therefore the bare Green's function reads:

$$G_0^+(\mathbf{r},\mathbf{r}';\omega^+) \equiv G_0^+(\mathbf{r}-\mathbf{r}';\omega^+) = \frac{1}{V}\sum_{\mathbf{k}}^{FBZ} G_0^+(\mathbf{k};\omega^+)e^{i\mathbf{k}\cdot(\mathbf{r}-\mathbf{r}')}$$
$$= \frac{1}{V}\sum_{\mathbf{k}}^{FBZ}\lim_{\eta\to\,0^+}\Big((\omega\pm i\eta) - \hat{H}_0(\mathbf{k})\Big)^{-1}e^{i\mathbf{k}\cdot(\mathbf{r}-\mathbf{r}')}.$$

After that, the Schrödinger equation is equivalent to the integral equations as already defined in eq.(1.6). Here we give the expression for the current bare propagator:

$$\psi(\mathbf{r}) = \int d^3\mathbf{r}' G_0^+(\mathbf{r}-\mathbf{r}';\omega^+)V(\mathbf{r}')\psi(\mathbf{r}')$$

where we have chosen the solution for bound states, since this is what we will be interested in the following.
As final outcome, we have derived an expression for Green's function $G_0^+(\omega)$ in terms of its free Hamiltonian $\hat{H}_0$. It follows the structure of $G_0^+(\omega)$ is strictly linked to the eigenvalues ω in the cases either they belong or they don't to the energy spectrum of $\hat{H}_0$.

1.2.3 Green's function of the scattering process: T-matrix method

Once the non-interacting part of the system is solved, next we want to examine the multiple elastic-scattering process over one static potential impurity at the origin of a regular lattice. Thus, we need to express the total Green's function $G^+(\omega)$ in terms of the bare Green's function $G_0^+(\omega)$ and $\hat{H}_{imp}$ impurity potential of the system, compare the scheme in fig.(1.5). Starting in **k**-representation and using eq.(1.5), the full propagator reads:

$$\begin{aligned} G^+(\mathbf{k},\mathbf{k}';\omega^+) &= \lim_{\eta\to\,0^+}\big[(\omega+i\eta)-\underbrace{(\hat{H}_0+\hat{H}_{imp})}_{\hat{H}}\big]^{-1} \\ &= \lim_{\eta\to\,0^+}\big[(\omega+i\eta-\hat{H}_0)(1-(\omega+i\eta-\hat{H}_0)^{-1}\hat{H}_{imp})\big]^{-1}. \end{aligned}$$

And we expand it in power series till we recognize the pattern of geometric series (we dropped the limit in η for the sake of clarity):

$$\begin{aligned} G^+(\mathbf{k},\mathbf{k}';\omega^+) &= \lim_{\eta\to\,0^+}\big[(1-(\omega+i\eta-\hat{H}_0)^{-1}\hat{H}_{imp})\big]^{-1}\underbrace{(\omega+i\eta-\hat{H}_0)^{-1}}_{G_0^+(\omega)} \\ &= \big(1+G_0^+H_{imp}+G_0^+H_{imp}G_0^+H_{imp}+...\big)G_0^+(\omega) \\ &= G_0^+(\omega)+G_0^+H_{imp}G_0^+(\omega)+G_0^+H_{imp}G_0^+H_{imp}G_0^+(\omega)+... \\ &= G_0^+(\omega)+G_0^+H_{imp}\underbrace{\big(1+G_0^+H_{imp}+G_0^+H_{imp}G_0^+H_{imp}+...\big)G_0^+(\omega)}_{G^+(\mathbf{k},\mathbf{k}';\omega)} \\ &= G_0^+(\omega)+G_0^+(\omega)\underbrace{H_{imp}\big(1-G_0^+H_{imp}\big)^{-1}}_{T(0;\omega)}G_0^+(\omega) \end{aligned}$$

where in the last line we have introduced an object called **T-matrix**. It has got the same analytical properties as the Green's function, namely by means of the complex plane it is analytic in all the plane excluding singularities on real axis. The position of those poles corresponds to the discrete energy spectrum of the Hamiltonian and viceversa. Next to the mathematical understanding we are going to complete soon, the T-matrix has an important role in scattering theory since it directly relates to both bare and full propagator. It includes all the dynamics of the scattering, what is happening to the particle from its first hit onto the impurity till it freely propagates again away from it. As earlier discussed, the impurity, due to its mass, causes only a variation to the propagation direction of the particle and thus, it carries no momentum i.e. $T(\mathbf{k}=0;\omega)$.
Going back to the expansion, we define the T-matrix of the process in momentum space as:

$$\boxed{T(0;\omega)\equiv\hat{H}_{imp}\big(1-G_0^+(\mathbf{k}_{int};\omega)\hat{H}_{imp}\big)^{-1}} \tag{1.7}$$

where $G_0^+(\mathbf{k}_{int};\omega)$ stands for the particle propagator freely moving from one scattering to the following on the impurity. Thus, it is given by the summation over all the internal momenta to the process, namely:

$$\sum_{k_n}G_0^+(k_n;\omega)=G_0^+(\mathbf{k}_{int};\omega).$$

The diagrammatic representation of the impurity scattering process is shown below.
Next, we expand the T-matrix in power series:

$$\begin{aligned} T(0;\omega) =& \hat{H}_{imp}\big(1-G_0^+(\mathbf{k}_{int};\omega)\hat{H}_{imp}\big)^{-1} \\ =& H_{imp}+H_{imp}G_0^+H_{imp}+H_{imp}G_0^+H_{imp}G_0^+H_{imp}+... \\ =& H_{imp}+H_{imp}\underbrace{\big(1+G_0^+H_{imp}+G_0^+H_{imp}G_0^+H_{imp}+...\big)G_0^+(\omega)}_{G^+(\mathbf{k},\mathbf{k}';\omega)}H_{imp} \end{aligned}$$

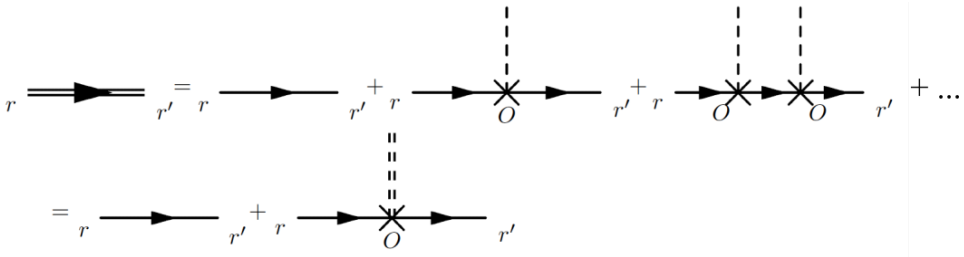

Figure 1.6: Feynman diagrams of impurity scattering in real space. The first line indicates the process given by the sum of the free propagation plus scattering over the impurity and its higher order scattering. In the second line, the summation of all the scattering processes is enclosed by the T-Matrix, that is represented by the double-dashed line.

and we reach a definition of it in terms of full propagator. Furthermore, such a definition allows to set a solid connection among the total Green's function $G^+(\omega)$, the bare Green's function $G_0^+(\omega)$ and $\hat{H}_{imp}$ impurity potential of the system.
The final expression of the total Green's function $G^+(\omega)$ is finally given by:

$$G^+(\mathbf{k},\mathbf{k}';\omega^+) = G_0^+(\mathbf{k};\omega) + G_0^+(\mathbf{k};\omega)T(0;\omega)G_0^+(\mathbf{k}';\omega)$$

and it matches the Feynman diagrams version of it, see figure.
A better understanding of the above terms is achieved by performing the Fourier transform of $G^+(\omega)$ to **r**-representation (for d-dimension):

$$G_0^+(\mathbf{r};\omega) = \int \frac{d^d\mathbf{k}}{(2\pi)^d} G_0^+(\mathbf{k};\omega)e^{i\mathbf{k}\cdot\mathbf{r}}$$

in order to get:

$$G^+(\mathbf{r},\mathbf{r}';\omega^+) = G_0^+(\mathbf{r}-\mathbf{r}';\omega) + G_0^+(\mathbf{r},0;\omega)T(0;\omega)G_0^+(0,-\mathbf{r}';\omega)$$
$$\text{with } T(0;\omega) \equiv \hat{H}_{imp}\left(1 - G_0^+(0;\omega)\hat{H}_{imp}\right)^{-1}.$$

In **r**-representation it is immediately displayed the lack of translationally invariance in the resulting full propagator due to the presence of the static impurity on the lattice. The bare propagators involved in the expression are still conserving the corresponding original momentum of the scattered particle. Next, the T-matrix is evaluated at impurity site - at the origin - as evidenced by the $G_0^+(0;\omega)$ which becomes a bare *local* propagator. Once we have calculated it, it turns out $T(0;\omega)$ has a crucial role. First, we have access to the full propagator of the scattering - hence, we can extract eigenvalues and eigenvectors of $\hat{H}$. Second, we have access to the local propagator $G_0^+(0;\omega)$ calculated at the impurity site - hence, from it we can describe wave function and energy levels of states located at the impurity (in particular, we will be interested in bound states).
The definition of the Green's function derived by means of T-matrix approach can be directly implemented in the integral equation eq.(1.6), i.e.:

$$\psi(\mathbf{r}) = \int d^3\mathbf{r}' G^+(\mathbf{r},\mathbf{r}';\omega^+)\hat{H}_{imp}\psi(\mathbf{r}'). \tag{1.8}$$

Since such an integral equation is equivalent to the original second order differential Schrödinger equation, from the knowledge of the Green's function we can ultimately derive an expression for the Hamiltonian of the system. This method is one of the key manipulation we will use in the following chapters.

As a conclusion of the paragraph, we add some comments on the kind of scattering we have been studying so far. For higher order of scattering, compare with the diagrams in the figure, we consider as a good approximation only events involving one impurity at the time. Thus,

neither two or more scattering on the same impurity nor crossing scattering between two different impurities. Under those conditions, we take an array of impurities and we can still treat them as if we were regarding many independent impurities put together. It follows the distances between them will play the important role to tune the scattering rate. The other variables, like the dimension or the strength of the impurity, will not much impact the scattering dynamics. Even more, in case we deal with not only nearest neighbor coupling but also with long-range impurity coupling.
A final comment is referred to the type of impurity: so far we have designed it as potential impurity approximated by a δ-Dirac attractive/repulsive potential. With this definition we will refer to both scalar impurity and magnetic one i.e. impurity that manifests a magnetic domain.

1.2.4 Bound states from scattering process

It has already been mentioned we are interested in **bound states** caused by the presence of impurities in the system. Aim of the section is to calculate the bare local propagator $G_0^+(0;\omega)$ of the T-matrix in order to find energy conditions to have such bound states in the system. A more detailed calculation is shown in Appendix (A).
We consider again a 1D regular lattice with one static non-magnetic impurity at the origin. To outline the procedure to find physical consistent energies, we select the expression of $G_0^+(0;\omega)$ for $\omega > 0$ and we plug it into the definition of the T-matrix eq.(1.7). Next, the energy values - corresponding to bound states located at the impurity sites - are going to be those which make the denominator of the T-matrix vanish, meaning:

$$T(0;\omega) = \frac{H_{imp}}{1 - G_0^+(0;\omega)H_{imp}} = 0 \iff 1 - G_0^+(0;\omega)H_{imp} = 0.$$

It is clear we seek for an expression of G_0^+. We start introducing the *spectral function* defined as the imaginary part of the full propagator, namely:

$$\begin{aligned}\varrho(\omega) &= -\frac{1}{\pi}\Im\Big[G^+(\mathbf{r},\mathbf{r}';\omega^+)\Big] \\ &= -\frac{1}{\pi}\Im\Big[G_0^+(\mathbf{r}-\mathbf{r}';\omega) + G_0^+(\mathbf{r},0;\omega)T(0;\omega)G_0^+(0,-\mathbf{r}';\omega)\Big].\end{aligned}$$

Great interest lies on the local bare propagator $G_0^+(0;\omega)$ contained in $\Im\Big[T(0;\omega)\Big]$, hence we have to calculate:

$$\Im\Big[\lim_{\eta\to\,0^+} G_0^+(0;\omega+i\eta)\Big] = \Im\int \frac{d\bar{\mathbf{k}}}{2\pi}\lim_{\eta\to\,0^+} G_0^+(0;\omega+i\eta)e^{i\bar{\mathbf{k}}\cdot 0}.$$

For positive ω, the outcome will be:

$$\begin{aligned}&1 - G_0^+(0;\omega)H_{imp} = 1 - \Big(-\sqrt{\frac{m}{2\omega}}\Big)H_{imp}^2 = 0 \\ &\Rightarrow \omega = \frac{mH_{imp}^2}{2}.\end{aligned}$$

We conclude, the energy values of bound states at the impurity are associated to the potential impurity itself of the system.
At first glance, this basic example shows the knowledge of $G_0^+(0;\omega)$ is indeed important to derive information about states localized at the impurity site.

1.3 Topological Classification

The present section introduces some basic concepts on topological invariant: we will address detailed discussion to those relevant concepts for the following chapters.

Additional reading can be found in Bernevig and Hughes [10], Hasan and Kane [12], Asbóth and Oroszlány [9].

Band structure can be classified by some topological invariant quantity. By invariance we mean theses quantities aren't modified if the Hamiltonian of the system undergoes to an *adiabatic deformation* - that is any continuous deformations which leave unchanged the number of occupied bands and their configuration. Thus, it is possible to make a topological classification of band structure until the energy gap closes. Indeed, gapless system results from a non-adiabatic deformation.
Topological invariant quantities identify the system phase, i.e. either topological or trivial, and generic properties under continuous deformations of the band structure.
There are two types of **topological invariant classifications** as follow:

- $\mathbb{Z}$-classification is defined by integer-value topological invariants and it can be used in system with broken time-reversal symmetry, in even dimension with gapped, non-trivial band structure. This invariance is called **Chern Number**. Systems with a non-trivial Chern Number, hence with values ± 1, are called **Chern Insulators**. As further reference, see Haldane paper [11].
- $\mathbb{Z}_2$-classification is defined by four topological invariant and it can be used in system with time-reversal symmetry, both odd and even dimension with non-trivial band structure. Systems under these conditions are called **Topological Insulators**. According to the value of the first invariant, we define either **strong** or **weak** topological insulator; compare with the chapter written by Moore in [14].

The next two sections will explain in a more detailed manner these classifications.

1.3.1 Chern Numbers and Chern Insulator

We start with a system whose energy spectrum is dispersive, thus it shows a non-trivial band structure. In general, any intrinsically nonmagnetic system in absence of an external magnetic field preserves *time-reversal symmetry*. Under these conditions, the *bulk bands* are gapless; hence their corresponding Hamiltonian is massless. If we break such a symmetry, the resulting Hamiltonian becomes massive and an energy gap appears in the bulk band structure. In case of non-trivial topological phase - we can detect that using an appropriate topological invariant - the system energy spectrum not only shows the non-trivial gapped bulk band but propagating gapless modes at the edge states - i.e. *chiral edge states*, see figure below. The chirality is due to the directness of each edge: backscattering processes are forbidden, since the counter-modes don't exist in each channel. Thus, edge states are robust to disorder.

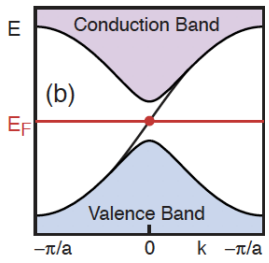

Figure 1.7: Scheme of energy spectrum in a Chern Insulator. Due to the broken time-reversal symmetry, the bulk bands are gapped. In a topological phase, gapless edge states will arise. [12]

System with broken time-symmetry and gapped bulk band structure can be distinguished according to $\mathbb{Z}$-classification: integer-value topological invariant n **Chern Numbers**. This

quantity is invariant in the sense it is robust to any adiabatic deformations - until gap closes and for the same number of occupied bands.
Originally, Chern Numbers can be understood by means of fiber bundles; however, it can be understood physically by introducing the concept of Berry's Phase.

Now, we shortly review the definition of **Berry's Phase**.
We start introducing a parameter space in terms of slowly varying parameters $\mathbf{R}(t) = (R_1, R_2, \cdots, R_N)$. Then, we introduce a general time-varying Hamiltonian $H(\mathbf{R}(t))$ in these parameters:

$$H(\mathbf{R}(t))|\psi(\mathbf{R}(t))\rangle = E_n(\mathbf{R}(t))|\psi(\mathbf{R}(t))\rangle$$

where we suppose the parameters are adiabatically evolving. Starting from the ground state $|\psi_0(\mathbf{R}(t))\rangle$ and studying the time evolution of the state, we find the basis functions are defined up to a phase:

$$|\psi(\mathbf{R}(t))\rangle = e^{i\theta(t)}|\psi_0(\mathbf{R}(t))\rangle = e^{i\gamma_n(t)}e^{-i\int_0^t E_n(\mathbf{R}(\mathbf{t}'))dt'}|\psi_0(\mathbf{R}(t))\rangle$$

where the system evolution is along a generic path $\mathcal{C}$.
Discussing the above expression, the second exponent indicates the dynamical phase depending on the time elapse. The first term is the geometrical phase:

$$\gamma_n(t) = \int_{\mathbf{R}(0)}^{\mathbf{R}(t)} \underbrace{\langle\psi_0(\mathbf{R}(t))|i\nabla_{\mathbf{R}}|\psi_0(\mathbf{R}(t))\rangle}_{\mathcal{A}(\mathbf{R})} \cdot d\mathbf{R}.$$

If we integrate $\gamma_n(t)$ over a closed contour $\mathcal{C}$, we obtain the definition of the Berry's phase. Over the same path the dynamical phase will vanish.
Using Stokes Theorem, the line integral over a closed contour is equivalent to the surface integral of $\mathcal{A}(\mathbf{R})$ - indeed called Berry's connection. The integral of the Berry's Flux - indeed called Berry's curvature - gives the Chern Numbers.
According to our interests, it is more relevant to discuss the actual formula of Chern Numbers in a two-band system, as we see next.

In a 2D system with broken time-reversal symmetry and two-band non-trivial structure, the Hamiltonian in momentum space assumes a quite compact form, the **Dirac Hamiltonian**, namely:

$$H_{\mathbf{k}} = \mathbf{d}(\mathbf{k}) \cdot \boldsymbol{\tau} = d_0(\mathbf{k})\mathbb{1} + d_x(\mathbf{k})\tau_x + d_y(\mathbf{k})\tau_y + d_z(\mathbf{k})\tau_z$$

that is a $2x2$ complex matrix with components in the Pauli matrices and identity bases.
That Hamiltonian allows a geometric interpretation - quite useful to understand the topological invariant too. The $\mathbf{d}(\mathbf{k})$-vector defines the mapping

$$\mathbf{d}(\mathbf{k}) : \mathbb{T}^2 \mapsto S^2.$$

The correspondence starts from a 2D Brillouin Zone. If we take periodic boundary conditions both in x- and y- directions, the BZ can be mapped to the surface of a torus. Next, we introduce the unit vector $\widehat{\mathbf{d}}(\mathbf{k}) = \dfrac{\mathbf{d}(\mathbf{k})}{|\mathbf{d}(\mathbf{k})|}$. Then, the surface of the torus is equivalent to the surface enclosed by the $\widehat{\mathbf{d}}(\mathbf{k})$-vector on a unit Bloch Sphere, see figure below. Hence, we start from a 2D space in terms of k_x, k_y components and we end up with a 3D unit vector spanning over a sphere.
By means of this geometric interpretation, the **Chern Numbers** of a gapped two-band system is defined as

$$n = \pm\frac{1}{4\pi}\int_{FBZ} d^2\mathbf{k} \quad \widehat{\mathbf{d}}(\mathbf{k}) \cdot \Big(\frac{\partial}{\partial k_x}\widehat{\mathbf{d}}(\mathbf{k}) \times \frac{\partial}{\partial k_y}\widehat{\mathbf{d}}(\mathbf{k})\Big)$$

and it counts the number of times the $\widehat{\mathbf{d}}(\mathbf{k})$-vector wraps around the unit sphere. This is why it is sometimes called *winding number*. Indeed, that number of times must be an integer

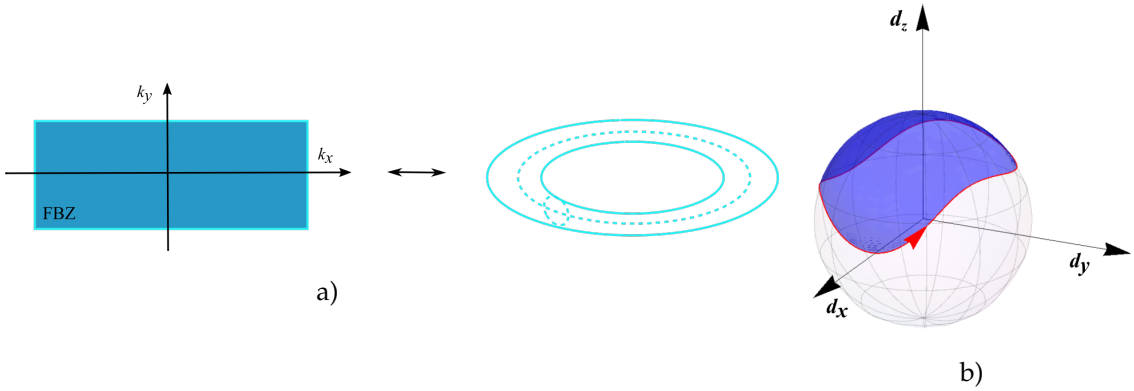

Figure 1.10: Map of the $\mathbf{d}(\mathbf{k})$: a) 2D First Brillouin Zone for x,y PBC is mapped to surface of torus. b) The unit vector wraps surfaces on the unit Bloch Sphere [9].

values of the covered area i.e. $4\pi n, n \in \mathbb{Z}$. And the signs is understood as the clockwise or anti-clockwise direction of winding over the sphere.
The Chern Numbers is a well-defined topological invariant for occupied, non-degenerate bands. In case of degenerate bands, only the summation of the Chern Numbers over all bands is still invariant, i.e. $\sum_{m=1}^{N} n_m = 0$ for N total bands.

As a conclusion, generic systems with broken time-reversal symmetry and gapped, non-trivial band structure are classified by the **Chern Numbers** of the occupied band:

- $n = 0$ indicates a trivial phase, hence a trivial insulator
- $n = \pm 1$ indicates a topological phase, hence **Chern Insulator**. This model has been first introduced by Haldane in 1988, [11].

As already remarked, the only way to go through one phase to another is passing through a gapless configuration.

1.3.2 Topological Insulator

The model of Chern Insulator exists only for even dimension. If we liked to study a similar system in 3D, we should switch to some different setting.
Since 2008, it has been discovered several 3D materials which exhibit topological phase in absence of an external magnetic field. These materials behave like an insulator in the bulk and like a metal on the surface, see previous energy bands scheme in fig.(1.3). This kind of material has been called **Topological Insulators**, since not only they differ from the Chern Insulator because of their availability in odd dimensions. They need to keep time-reversal symmetry in order to preserve edge states, hence these states are topologically protected, see again Moore [14] and [13].
In presence of time-reversal symmetry, the Chern Numbers vanish, hence the $\mathbb{Z}$-classification isn't suitable any more. We introduce an additional classification, the $\mathbb{Z}_2$-classification: it is defined by a set of four invariants $(\nu_0; \nu_1, \nu_2, \nu_3)$ over the occupied bands. The first term indicates the case either strong $\nu_0 = 1$ or weak $\nu_0 = 0$ Topological Insulator. The remaining terms approximately stand for the three directions in space, if we consider a 3D Topological Insulator.
According to our purposes, the observable feature of these systems is the metallic surface. Particularly, we study the surface energy spectrum, that is generically described by a massless Hamiltonian. We define by *Dirac point* $\mathbf{k}_F$ a Fermi surface shrank from a circle to a point. In case a Fermi surface is enclosing an odd number of Dirac points, we have a 3D strong Topological Insulator. If it is an even number, it results a weak topological insulator. Since the energy is linear in momentum, the corresponding energy dispersion assumes the typical

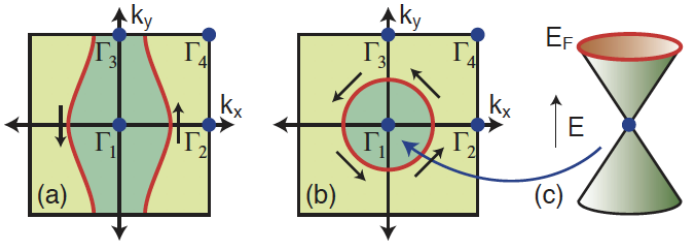

Figure 1.11: On the left, an even number of enclosed Dirac points by a Fermi surface leads to a weak topologiocal insulator. On the right, an odd number of enclosed Dirac points indicate the system is a 3D strong TI. Its energy spectrum has the typical Dirac cone dipersion. [12]

cone shape i.e. the spectrum is a *Dirac cone*, see the figure.
As a general property, a strong topological insulator has an odd number of Dirac cones on each surface. However, this doesn't violate the fermion doubling theorem since each cone has its own partner on the opposite surface. Thus, it is still valid that in a time-reversal symmetry system the Dirac points come in pairs always. Moreover, each surface can be regarded as half an ordinary metal - again taking in consideration both surfaces we gain back the metallic states typical of Topological Insulators.

As a conclusion, we cite some material considerations concerning Topological Insulator [15]. The first candidates were semiconductors and semimetal: indeed, the very first experimental evidence of TI was in the alloy $Bi_{1-x}Sb_x$ (2008). Its metallic surface states have been mapped by angle resolved photoemission spectroscopy (ARPES). Actually, this material isn't the most appropriate because its surface band is quite complicated.
A second-generation of material has been discovered in Bi_2Se_3 - with a bandgap of 0.3eV and Bi_2Te_3 - with a bandgap of 0.15eV. In this case, the topological phases can be detected easily. However, it is difficult to investigate transport properties of the system because of the high degree residual bulk conductivity.
A completely different approach is achieved by semimetal in crystal form like 3D strain of $HgTe$.

Chapter 2

The Model

The background of our project is the paper *Topological state engineering by potential impurities on chiral superconductors* [16] - based on an impurity lattice deposited on the top surface of a p-wave superconductor. What triggers our interest is that from the designed system - studied in an effective-model - they found Chern Numbers integer invariant at high values, i.e. up to 60.
However, p-wave superconductors aren't yet experimentally well established. The lack of practical possibility to a physical realization of the model with superconductor suggests us a different basement. We decide to use a 3D Topological Insulator (3D TI). Indeed, we have a quite large choice of materials to implements TI. Starting from the very first 3D TI to be experimentally identified, the semiconducting alloy $Bi_{1-x}Sb_x$ in 2008. Then, a second generation of 3D material has been discovered in Bi_2Se_3, Bi_2Te_3. Another option is given by the 3D strain $HgTe$.
Motivated by all that, this chapter presents the setting of system we want to study - top surface of 3D strong topological insulator with a lattice of impurity - by introducing its effective two-band model in order to find an analytical expression for an effective Hamiltonian describing the setting.
Our ultimate goal is to evaluate the Chern Numbers of the occupied bands created by the array of impurity and see what response the system has. That will be presented in the next chapter, where the features of the model will be described.

2.1 The 1D Effective-Model

The physics behind the model we want to study is completely manifested if we consider its **effective-model**.
We start studying a system with 1D gas of non-interacting spinless electrons, very dense - it means the lattice constant a_{elec} is tiny. Hence, this layer is regarded as a continuum and it is described by the Hamiltonian $\hat{H}_0$. In the center of it, we locate a unique impurity with the following properties. It is neither charged nor magnetic type, it is *static* - $M_{imp} \gg m_{elec}$, *structureless* - it possesses only translational internal degree of freedom thus guarantee of *elastic scattering*, its spectrum has got one energy level. The presence of the impurity breaks the translationally invariance of the original continuum system and we define it by a delta-Dirac potential in $\hat{H}_{imp}$
We introduce the Hamiltonian of the system in first quantization:

$$\hat{H} = \hat{H}_0 + \hat{H}_{imp} = -\frac{\hbar^2}{2m_{elec}}\partial_x^2 + V\delta(x), \tag{2.1}$$

with V strength of the impurity. The elastic scattering dynamics is the same we introduced in Chapter 1, meaning the process is well-described by the *T-Matrix*, namely:

$$T(0;\omega) = V(1 - \sum_i G_0^+(k_i;\omega)V)^{-1}$$

where the summation refers to all the internal momenta involved into the scattering process. Then, the bare propagator reads:

$$\begin{aligned} &G_0^+(x,x';\omega) \equiv G_0^+(x-x';\omega) = \lim_{\eta\to\,0^+} G(\omega \pm i\eta) = \lim_{\eta\to\,0^+} \left((\omega \pm i\eta) - \hat{H}_0\right)^{-1} \\ &\to G_0^+(x-x';\omega) = \frac{1}{\sqrt{L}} \int \frac{dk}{2\pi} G_0^+(k;\omega) e^{-ik(x-x')}. \end{aligned} \tag{2.2}$$

As evidence of it, the original continuum 1D system satisfies conservation of momentum. Next, we introduce the time-independent Schrödinger equation of the system:

$$\hat{H}\psi = E\psi \quad \Rightarrow \quad (E - \hat{H}_0)\psi = \hat{H}_{Imp}\psi. \tag{2.3}$$

As already discussed, that equation is equivalent to the integral equation:

$$\begin{aligned} \psi(x) &= \int dx' G_0^+(x-x';\omega)\hat{H}_{Imp}(x')\psi(x') \\ &= \int dx' G_0^+(x-x';\omega) V\delta(x')\psi(x') \\ &\Rightarrow \psi(x) = V G_0^+(x;\omega)\psi(0). \end{aligned} \tag{2.4}$$

According to the position in the origin of the impurity, we can rewrite the integral equation into

$$(1 - V G_0^+(x;\omega))\psi(0) = 0 \tag{2.5}$$

that is an eigenvalues equation for eigenvalue 1 and eigenvectors

$$\psi(0) = \begin{pmatrix} \psi_1(0) \\ \psi_2(0) \end{pmatrix} \quad , \quad \text{with } \psi_1(0) = \begin{pmatrix} 1 \\ 0 \end{pmatrix} \text{ and } \psi_2(0) = \begin{pmatrix} 0 \\ 1 \end{pmatrix}.$$

To get closer to the actual conditions we want to study, we implement a 1D effective-model with the same conditions just discussed but placing on the layer a lattice of impurity with the same properties as before. This 1D chain is rarefied i.e. $a_{imp} \gg a_{elec}$ and isotropic. The layer including the impurity lattice has restored translationally invariant. Each impurity can be regarded as independent, as if we had grouped in a close configuration impurities which were originally at distance from one to another. However, their outer orbitals have a tiny probability to tunnel from one site to the next one. From those overlaps, a non-trivial electronic band structure arises. Having that, we can classify the bands according to some integer values topological invariant, i.e. Chern Numbers.
We introduce again the Hamiltonian of the system in first quantization for N- lattice sites:

$$\hat{H} = -\frac{\hbar^2}{2m_{elec}}\partial_x^2 + V\sum_{n=1}^{N-1}\delta(x - x_n). \tag{2.6}$$

Now, following the way we presented the T-matrix, in the case of multiple impurities we don't allow neither two or more scattering on the same impurity nor cross scattering between two different impurities. Thus, even for higher order of scattering, we regard as a good approximation only events involving one impurity at the time. However, according to the property of the impurity sublattice, such T-matrix approach is not efficient any more. Hence, we can apply then the Green's function method to derive an equivalent integral equation to solve the Schrödinger equation of the system:

$$\begin{aligned} \psi(x_m) &= \int dx' G_0^+(x_m - x';\omega) V \sum_{n=1}^{N-1}\delta(x' - x_n)\psi(x') \\ \Rightarrow \psi(x_m) &= V\sum_{n=1}^{N-1} G_0^+(x_m - x_n;\omega)\psi(x_n), \end{aligned} \tag{2.7}$$

where N indicates the number of impurities in the lattice.
Next, we think of the wave function $\psi(x_m)$ as a component of a general *wave vector* acting on $mth-$impurity, namely:

$$\overrightarrow{\Psi} = \begin{pmatrix} \psi(x_1) \\ \psi(x_2) \\ \vdots \\ \psi(x_n) \end{pmatrix}$$

for $n = 1, ..., N-1$. Hence, we can define an integral equation in terms of the wave vector and the distance $X_{nm} = a_{imp}(x_m - x_n)$ between two impurities as follow:

$$\overrightarrow{\Psi} = VG_0^+(X_{nm};\omega)\overrightarrow{\Psi} \iff \Big(\mathbb{1} - VG_0^+(X_{nm};\omega)\Big)\overrightarrow{\Psi} = 0 \tag{2.8}$$

where we recognize again an eigenvalues equation for eigenvalue 1 and eigenvector $\overrightarrow{\Psi}$.
Rewriting the time-independent Schrödinger equation using the wave vector $\overrightarrow{\Psi}$ and the previous integral expression:

$$\begin{aligned} E\mathbb{1}\overrightarrow{\Psi} &= H\overrightarrow{\Psi} \\ &= (\hat{H}_0 + \hat{H}_{Imp})\overrightarrow{\Psi} \\ &= \Big(E\mathbb{1} + 1 - VG_0^+(X_{nm};\omega_0)\Big)\overrightarrow{\Psi} \\ &= f(E)\overrightarrow{\Psi} \end{aligned}$$

where $f(E) = (E-1)\mathbb{1} + VG_0^+(X_{nm};\omega_0)$ is an exact expression as a function of energy. Here, we need to introduce a two-steps approximation in order to connect our result to an effective equation. First, the energy range must be quite small. Next, we assume the energies involved in the Green's function are close to the eigenenergies ω_0. Hence, we get:

$$\begin{aligned} &E\mathbb{1}\overrightarrow{\Psi} = (\hat{H}_0 - \hat{H}_{Imp})\overrightarrow{\Psi} \quad \rightarrow \quad E\mathbb{1}\overrightarrow{\Psi} = \Big((\omega_0 - 1)\mathbb{1} + VG_0^+(X_{nm};\omega_0)\Big)\overrightarrow{\Psi} \\ &\Rightarrow \boxed{\hat{H}_{nm} = (\omega_0 - 1)\delta_{nm} + VG_0^+(X_{nm};\omega_0)}. \end{aligned} \tag{2.9}$$

where in the last line we indicate the expression for the **effective Hamiltonian** $\hat{H}_{nm}$ that describes the full lattice system. Assuming periodic boundary conditions, its matrix structure reads:

$$\hat{H}_{nm} = \begin{pmatrix} \omega_0 - 1 + VG_0^+(0;\omega_0) & VG_0^+(X_{nm};\omega_0) & VG_0^+(2X_{nm};\omega_0) & \dots & (VG_0^+(0;\omega_0))^\dagger \\ (VG_0^+(X_{nm};\omega_0))^\dagger & \omega_0 - 1 + VG_0^+(0;\omega_0) & VG_0^+(X_{nm};\omega_0) & \dots & \vdots \\ (VG_0^+(2X_{nm};\omega_0))^\dagger & (VG_0^+(X_{nm};\omega_0))^\dagger & \omega_0 - 1 + VG_0^+(0;\omega_0) & \dots & \vdots \\ \vdots & \vdots & \vdots & \ddots & \\ \vdots & \vdots & \vdots & \vdots & \ddots \\ \omega_0 - 1 + VG_0^+(0;\omega_0) & \dots & \dots & \dots & \omega_0 - 1 + VG_0^+(0;\omega_0) \end{pmatrix}. \tag{2.10}$$

We pause here with some comments on the matrix before moving on. The main diagonal describes the scattering process over a single impurity at the center of the layer. The first upper diagonal - matrix elements like $g_{1,m+1}$ - indicates the nearest-neighbor scattering, hence the Green's function $\propto X_{nm}$. The adjacent diagonal - matrix elements like $g_{1,m+2}$ - indicates the next-nearest-neighbor scattering, hence the Green's function $\propto 2X_{nm}$. The trend is quite clear, and lower diagonals with respect to the main one are just the adjoint elements. Due to periodic boundary, top right corner g_{1m} is equal to bottom left one g_{n1}.
Without loss of generality, we consider interactions between the nearest neighbor (NN) only. Hence, only the main diagonal, the one referring to $g_{1,m+1}$, its adjoint and the elements

g_{1m}, g_{n1} aren't zero.
Now, we move a step further. We proceed switching to second quantised formalism by introducing fermionic spinless operator $c_i^\dagger, c_i$ - creation and annihilation at lattice site i respectively. According to such a formalism, it turns out we can make a very instructive analogy.
On one side we have derived an effective-lattice model for a *multiple impurity array* over a 1D layer. We end up with the matrix elements of the effective Hamiltonian in terms of the local bare Green's function - describing the scattering process.
On the other side, analysing the energy spectrum of the multiple impurity we find *electronic bands*. We know already such a kind of structure can be described by a *Tight-Binding approximation* - with a characteristic t_{ij} strength of the hopping amplitude of electrons.
And so, under the second quantised frame, we can identify the matrix elements of Green's function with the hopping terms, namely:

$$\boxed{t_{ij} \equiv G_0^+(X_{ij};\omega_0) = G_0^+(x_i - x_j;\omega_0)}.$$

The lattice version of the effective-model we have derived so far, not only it allows the analogy but it is ideal to describe topological properties of bands structure - as we will see next.
Then, recalling the discussion in Chapter 1, we are ready to write down the Tight-Binding Hamiltonian for NN-hopping in 1D real space:

$$H = \sum_{i=1}^{N} \epsilon_0 c_i^\dagger c_i - \sum_{i=1}^{N-1} \Big(t c_i^\dagger c_{i+1} + t^\star c_{i+1}^\dagger c_i \Big), \tag{2.11}$$

where we have evaluated the second summation $< ij >$ for NN thus $t_{ij} \equiv t$ and $t = t^\star$ for real matrix elements.
Going to momentum space, we perform the Fourier transform and we obtain:

$$H_k = \sum_k a_k^\dagger (\epsilon_0 + 2t\cos(ka)) a_k = \sum_k a_k^\dagger \epsilon_k a_k \tag{2.12}$$

with

$$\epsilon_0 = \omega_0 - 1 + V G_0^+(0;\omega_0) \text{ and } t = V G_0^+(X_{nm};\omega_0)$$

where ϵ_k is the energy dispersion of the system in terms of the single-particle energy ϵ_0 and the local bare Green's function.

2.2 The Effective-Model of the surface of 3D Strong Topological Insulator

By expanding the previous model to a 2D version, the same strategy can be used to define an **effective two-band model** for one **surface of a strong 3D topological insulator** (3D TI). The setting is the following:

- the 3D bulk that is an insulator is referred to the basement i.e. the volume of the 3D TI. According to the design of the system, the bulk makes no contribution to what is happening on the surface. Its energy bands are flat in comparison to the energy spectrum we will build on its surface. The two surfaces are considered as infinitely distant - thus no link among them - and we study only the top one, say on xy-plane. Then we know k_x, k_y are good quantum numbers to write down equations.

- the free-particle like Hamiltonian is referred to the top surface of the TI, that is the part of the system we actually study. It can be regarded as a very dense lattice - a continuum system. We assume the chemical potential, term like $\mathbb{1}\mu$, is set to zero. Hence, the *Surface Hamiltonian* reads:
$\hat{H}_{\mathbf{k}}^{Surface} = \hbar v_F(-i\overrightarrow{\partial} \cdot \overrightarrow{\tau})$, with $\overrightarrow{\tau} = (\mathbb{1}, \tau_x, \tau_y, \tau_z)$ unit matrix and Pauli matrices respectively.

- breaking the time-reversal symmetry of the top surface means the surface Hamiltonian becomes massive by adding a *mass* term $|M|\tau_z$. The effect on the surface energy spectrum is the appearance of an *energy gap*. The mass term will impose the energy scale of the system, thus within that range we want to create a non-trivial band structure - and later it will be classified by some topological invariant.
- on the top of the surface we place an impurity lattice - each is static, structureless, with two energy levels which are chosen in the middle of the gap range. The very general form of the *Impurity Hamiltonian* is defined by:
  $\hat{H}_{imp}(\mathbf{r}) = \sum_i \overrightarrow{V} \cdot \overrightarrow{\tau}\delta(\mathbf{r}-\mathbf{r}_i)$, with the strength V takes into account both the scalar $V_0\mathbb{1}$ and magnetic $V_M\tau_z$ impurity case.

Hence, according to such a setting, we will derive an **effective lattice model** of the surface of 3D Strong TI.
We start again with the case of one impurity situated at the center on the top surface.
The way we introduced the setting is in first quantisation formalism. It is convenient to switch to second quantisation by means of the spinor acting on the impurity site:

$$\Psi^\dagger_{\mathbf{k}} = \begin{pmatrix} \psi^\dagger_{\mathbf{k}} \\ \psi_{\text{-}\mathbf{k}} \end{pmatrix}.$$

Using their Fourier Transform:

$$\Psi(\mathbf{r})^\dagger = \int \frac{d\mathbf{k}}{(2\pi)} \Psi^\dagger_{\mathbf{k}} e^{-i(\mathbf{k}\cdot\mathbf{r})},$$

we present the second quantized Hamiltonian in momentum space, namely:

$$\hat{H}_{\mathbf{k}\mathbf{k}'} = \hat{H}^{Surface}_{\mathbf{k}} + \hat{H}^{Imp}_{\mathbf{k}\mathbf{k}'} = \int \frac{d^2\mathbf{k}}{(2\pi)^2} \Psi^\dagger_{\mathbf{k}} \Big(\hbar v_F \mathbf{k}\cdot\overrightarrow{\tau}\Big)\Psi_{\mathbf{k}} + \int \frac{d\mathbf{k}}{(2\pi)} \int \frac{d\mathbf{k}'}{(2\pi)} \Psi^\dagger_{\mathbf{k}} \Big(\overrightarrow{V}\cdot\overrightarrow{\tau}\Big)\Psi_{\mathbf{k}'}, \tag{2.13}$$

where the final system has lost the translational invariant property.
In real space, the time-independent Schrödinger equation reads:

$$\Big(E - \hat{H}^{Surface}(\mathbf{r})\Big)\Psi(\mathbf{r}) = \overrightarrow{V}\cdot\overrightarrow{\tau}\Psi(\mathbf{r}) \tag{2.14}$$

that is equivalent to solve

$$\Psi(\mathbf{r}=0) = \overrightarrow{V}\cdot\overrightarrow{\tau}G^+_0(\mathbf{r}=0;E)\Psi(\mathbf{r}=0) \tag{2.15}$$

where the local bare propagator can be derived from the knowledge of the T-matrix, hence from the surface masseless Hamiltonian.

As final implementation, we can write the effective-two band-model of the top surface of 3D TI in condition of broken time-reversal symmetry. In addition, we locate a square array of impurity. That array is isotropic and rarefied according to the length scale of the bulk, i.e. $a_{Imp} \gg a_{bulk}$. Each impurity shows two discrete non-degenerate energy levels which will result into in-gap bound states. The collection of impurity will create band structure whose bandwidth is tuned withing the energy gap.
The top surface - the only part of the system we are actually interested in - is made up by the overlap of two sub-lattices. The discrete lattice of impurity is surrounded by the dense underneath original lattice. Hence, that global 2D structure shows again momentum conservation.
For N-impurity, the integral equation equivalent to the Schrödinger one is defined by Green's function method, namely:

$$\Big(E - \hat{H}^{Surface}(\mathbf{r})\Big)\Psi(\mathbf{r}) = \sum_{i=1}^{N} \overrightarrow{V}\cdot\overrightarrow{\tau}\delta(\mathbf{r}-\mathbf{r}_i)\Psi(\mathbf{r}) \quad \Leftrightarrow \quad \Psi(\mathbf{r}) = \overrightarrow{V}\cdot\overrightarrow{\tau}\sum_{i=1}^{N}\delta(\mathbf{r}-\mathbf{r}_i)G^+_0(\mathbf{r}-\mathbf{r}_i;E)\Psi(\mathbf{r}_i), \tag{2.16}$$

where $\Psi(\mathbf{r})$ is the spinor acting on the impurity sub-lattice, hence it acts on the location of the impurity site in the square lattice.
In order to make possible such kind of equivalence, we had to applied the two-steps approximation as we encountered already in the 1D case. First, we expand the energy within the limit $|E| \ll |M| \ll D_{Bulk}$, where $D_{Bulk} = v_F \times \Lambda$ is the bulk bandwidth in terms of the Fermi velocity and the energy Λ. The latter identifies the energy level of valence/conduction bulk bands (in the following, this energy will be used as cut-off to avoid UV divergences in integral evaluations). Secondly, we assume the energies involved in the Green's function are close to the in-gap bound states eigenenergies E_{BS}.
Next, thinking of $\Psi(\mathbf{r})$ as a wave vector as in the 1D case, we can express the eigenvalues equation into:

$$E\Psi(\mathbf{r}) = \hat{H}\Psi(\mathbf{r}) = \begin{cases} \Big(E_{BS} - 1 + \overrightarrow{V} \cdot \overrightarrow{\tau} G_0^+(0; E_{BS})\Big)\Psi(\mathbf{r}) & \text{if } \mathbf{r} = \mathbf{r}' \\ \overrightarrow{V} \cdot \overrightarrow{\tau}\, \delta(\mathbf{r} - \mathbf{r}') G_0^+(\mathbf{r} - \mathbf{r}'; E_{BS})\Psi(\mathbf{r}') & \text{if } \mathbf{r} \neq \mathbf{r}' \end{cases}, \tag{2.17}$$

where E_{BS} is the bound states energy. In the above expression, the first case indicates the setting of one impurity placed at the center of the surface. Thus, the matrix of such a Hamiltonian will display only the main diagonal, all the other elements will vanish. The second case refers to the setting with a square array of impurity on the surface. Here the matrix Hamiltonian will show the full structure - similar to the 1D case we wrote before.
As a final conclusion, we can make the same analogy between Tight-Binding approximation for band structure and the local bare Green's function for a system regarding any order of hopping process i.e. not only a nearest-neighbor coupling but a long-range coupling too. We introduce 2D fermionic spinless operator $c_{ij}^\dagger$ and c_{ij} - creation and annihilation on the lattice site $\mathbf{r}_i = a_{Imp} \begin{pmatrix} i \\ j \end{pmatrix}$ respectively.
The 2D Hamiltonian in real space reads:

$$\begin{aligned} H &= \frac{1}{2} \sum_{ii',jj'} \left(t_{ii',jj'} c_{ij}^\dagger c_{i'j'} + t_{ii',jj'}^\star c_{i'j'}^\dagger c_{ij} \right) \\ &= \sum_{ij} t_0 c_{ij}^\dagger c_{ij} + \sum_{ii',jj'} t (c_{ij}^\dagger c_{i'j'} + c_{i'j'}^\dagger c_{ij}), \end{aligned} \tag{2.18}$$

where

$$t_0 \equiv G_0^+(0; E_{BS}) \quad , \quad t \equiv G_0^+(\mathbf{r} = \mathbf{r}_i - \mathbf{r}_j; E_{BS}) \quad \text{for } t \in \mathbb{R}.$$

We note, once the energy scale is set by assigning a value to the mass term, the only tuneable parameter is the path between consecutive hopping i.e. the Green's function depends on the difference $\mathbf{r}_i - \mathbf{r}_j$.
For practical purposes, it is useful to have the momentum space version of the Hamiltonian, since the final effective Hamiltonian in that space has a suitable form we can easily employ to calculate the Chern Numbers of the gapped band structure.
In the Appendix (B), as an introductory study to Chapter 3, it is shown the 2D Fourier Transform for Nearest-Neighbor hopping only.

2.3 Towards the Effective-Model

By now, the general structure of the system has been defined: we can go into some more details of it. For practical reasons, we assume natural unit i.e. $\hbar = 1$ and $v_F = 1$ Fermi velocity.
The basement of the system is a 3D Strong Topological insulator, it plays the role of bulk in the model. The family of materials and heterostructures can host surface metallic states and be an insulator in the bulk is quite big. Starting from the original bismuth alloy Bi_xSb_{1-x} discovered in 2008 to some more recent type like 3D strain of $HgTe$, they are all suitable to implement our model in an experiment.

We dispose close to the top surface a ferromagnetic material - like iron, cobalt or nickel - to induce the gap in the surface energy spectrum.
Then, a lattice of impurity is deposited only on the top surface. We decide to engineering the impurity as a mix of both scalar and magnetic type. However, the latter could be already by itself a source to open a gap into the band structure. We assume the strength of the magnetic impurity will never be so strong to actually create the gap. Moreover, the lattice is designed in a square configuration and isotropic. Eventually, such an arbitrary configuration will not affect the outcome.

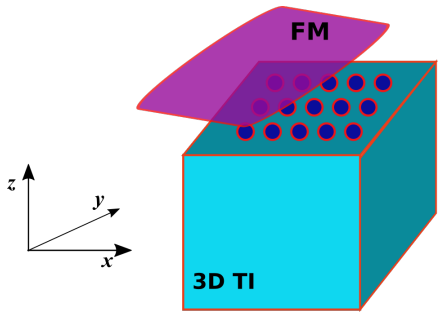

Figure 2.1: Sketch of the setting.

We introduce the 2D Hamiltonian of system. The surface massive Hamiltonian is defined by:

$$\hat{H}_{\mathbf{k}}^{Surface} = v_F(k_x\tau_x + k_x\tau_x) + |M|\tau_z \tag{2.19}$$

and the lattice Hamiltonian for N impurity

$$\hat{H}(\mathbf{r})^{Imp} = \sum_{i=1}^{N}(V_0\mathbb{1} + V_M\tau_z)\delta(\mathbf{r}-\mathbf{r}_i) \Rightarrow \quad \hat{H}_{\mathbf{k}\mathbf{k}'}^{Imp} = \int \frac{d\mathbf{k}}{(2\pi)} \int \frac{d\mathbf{k}'}{(2\pi)} \Psi_{\mathbf{k}}^{\dagger}\Big(V_0\mathbb{1} + V_M\tau_z\Big)\Psi_{\mathbf{k}'}, \tag{2.20}$$

where we have used the Fourier Transform

$$\psi_{\mathbf{k}} = \int \frac{d^2\mathbf{k}}{(2\pi)^2}\psi(\mathbf{r})e^{i\mathbf{k}\cdot\mathbf{r}}.$$

The general strategy we adopt to calculate an expression for the effective Hamiltonian runs as follow.
We start with the **time-independent Schrödinger equation** in real space, namely:

$$(E - \hat{H}(\mathbf{r})^{Surface})\psi(\mathbf{r}) = \hat{H}(\mathbf{r})^{Imp}\psi(\mathbf{r}).$$

We already know, see eq.(1.6), we can write the **integral equation** equivalent to the second order differential Schrödinger equation:

$$\psi(\mathbf{r}) = \hat{H}(\mathbf{r})^{Imp}\mathcal{G}_0^{+}(\mathbf{r};E)\psi(\mathbf{r}). \tag{2.21}$$

For such an equation, the corresponding retarded Green's functions in momentum space, see eq.(1.5), are defined as:

$$G^{+}(\mathbf{k},\mathbf{k}';E) = \lim_{\eta\to\,0^+}\left((E+i\eta) - \hat{H}_{\mathbf{k}\mathbf{k}'}^{Imp}\right)^{-1} \quad ; \quad G_0^{+}(\mathbf{k};E) = \lim_{\eta\to\,0^+}\left((E+i\eta) - \hat{H}_{\mathbf{k}}^{Surface}\right)^{-1}$$

and they satisfy, see eq.(1.4):

$$\Big(E - \hat{H}_{\mathbf{k}\mathbf{k}'}^{Imp}\Big)G^{+}(\mathbf{k},\mathbf{k}';E) = \mathbb{1} \quad ; \quad \Big(E - \hat{H}_{\mathbf{k}}^{Surface}\Big)G_0^{+}(\mathbf{k};E) = \mathbb{1}.$$

In the following, we refer to the Green's function $\mathcal{G}_0^{+}(\mathbf{r};E)$ the expression:

$$\mathcal{G}_0^{+}(\mathbf{r};E) = \lim_{\eta\to\,0^+}\mathcal{G}_0(\mathbf{r};E+i\eta).$$

In the case of one unique impurity in the system, we can employ the T-matrix method - see eq.(1.7):

$$T(0;E) = \hat{H}^{Imp}_{\mathbf{k}\mathbf{k}'}\left(1 - \mathcal{G}^{+}_{0}(\mathbf{k};E)\hat{H}^{Imp}_{\mathbf{k}\mathbf{k}'}\right)^{-1},$$

in case of multiple impurity we use Green's function methods only.
The next paragraphs are dedicated to compute an analitycal expression for the Green's function:

$$\begin{aligned}\mathcal{G}^{+}_{0}(\mathbf{k};E) &= \lim_{\eta \to 0^{+}} \Big((E + i\eta) - (v_F(k_x\tau_x + k_y\tau_y) + M\tau_z) \Big)^{-1} \\ &= \frac{1}{E^2 - M^2 - v_F^2 \underbrace{(k_x^2 + k_y^2)}_{|\mathbf{k}|^2}} \begin{pmatrix} E + M & v_F(k_x - ik_y) \\ v_F(k_x + ik_y) & E - M \end{pmatrix}. \end{aligned} \tag{2.22}$$

We extensively use this latter expression to finalize the calculation.
In order to compute an actual form, we start with case of a unique impurity located at the center, after we think of many of those grouped together in order to end up with a band structure. Once we obtain those forms, the Green's functions can be filled into the integral equations. These are equivalent to the original Schrödinger equation. Therefore, we can read off an expression of the effective Hamiltonian from it - in real space.

2.4 Single Impurity Model

In the section we compute $\mathcal{G}^{+}_{0}(\mathbf{r} = 0; E)$ for one impurity and find an expression for energy levels of the bound states caused by its presence.

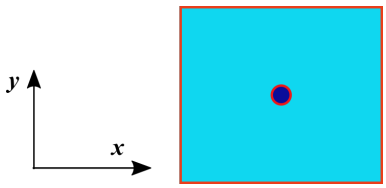

Figure 2.2: Sketch of one impurity setting.

The integral equation, given in eq.(2.21), now reads:

$$\psi(0) = \hat{H}^{Imp}\mathcal{G}^{+}_{0}(0;E)\psi(0) \iff \Big(\mathbb{1} - \hat{H}^{Imp}\mathcal{G}^{+}_{0}(0;E)\Big)\psi(0) = 0.$$

The case treats a single impurity, hence the T-matrix is an ideal approach. The local bare propagator in real space is given by:

$$\mathcal{G}^{+}_{0}(0;E) = \int \frac{d^2\mathbf{k}}{(2\pi)^2}\mathcal{G}^{+}_{0}(\mathbf{k};E)e^{-i\mathbf{k}\cdot 0}.$$

The matrix form of the Green's function:

$$\mathcal{G}^{+}_{0}(0;E) = \begin{pmatrix} X_0(0) + X_1(0) & X_2^{+}(0) \\ X_2^{-}(0) & X_0(0) - X_1(0) \end{pmatrix}$$

where the elements - recalling $\mathcal{G}^{+}_{0}(\mathbf{k};E)$ in eq.(2.22) - are defined as:

$$\begin{aligned} X_0(0)\mathbb{1} &= (E\mathbb{1}) \int_0^{\Lambda} \frac{d^2\mathbf{k}}{(2\pi)^2} \frac{1}{E^2 - M^2 - v_F^2|\mathbf{k}|^2} \\ X_1(0)\tau_3 &= (M\tau_3) \int_0^{\Lambda} \frac{d^2\mathbf{k}}{(2\pi)^2} \frac{1}{E^2 - M^2 - v_F^2|\mathbf{k}|^2} \\ X_2^{\pm}(0)(\tau_1 + \tau_2) &= \int_0^{\Lambda} \frac{d^2\mathbf{k}}{(2\pi)^2} \frac{k_x \pm ik_y}{E^2 - M^2 - v_F^2|\mathbf{k}|^2}. \end{aligned}$$

where we had to use the cut-off Λ up to the first Brillouin zone since the integrals show a UV-divergence. Solving in polar coordinates and we obtain:

$$X_{0,1}(0) = \frac{1}{4\pi}\int_0^{\Lambda} \frac{d(k^2)}{(E^2-M^2)/v_F^2 - k^2} = -\frac{1}{4\pi}\log\left(\frac{(E^2-M^2)/v_F^2 - \Lambda^2}{(E^2-M^2)/v_F^2}\right) = -\frac{1}{4\pi}\log\left(1 - \frac{\Lambda^2}{(E^2-M^2)/v_F^2}\right)$$

whereas $X_2^{\pm}(0)$ vanish due to the symmetry of their angular part.
Hence we result into the expression:

$$\mathcal{G}_0^+(0;E) = -\frac{1}{4\pi}\begin{pmatrix} E-M & 0 \\ 0 & E+M \end{pmatrix}\log\left(1 - \frac{\Lambda^2}{(E^2-M^2)/v_F^2}\right).$$

A first comment on the local bare propagator. Even though Λ fixes the general available energy range, it is the mass term that actually dictates the boundary. According to such an energy scale, i.e. $E < |M| \ll D_{Bulk}$, we need to apply some constraints to energies. They have to be evaluated within the mass term M: such a restriction guarantees the bound state energy levels inside the energy gap - possibly at the center of it. This latter condition will turn essential to derive an effective equation. Given these assumptions, we Taylor expand the logarithm in first order and we get the final expression for the **local bare propagator for single impurity bound states**:

$$\boxed{\mathcal{G}_0^+(0;E) = -\frac{1}{4\pi}(E\mathbb{1} + M\tau_3)\log\left(1 + \left(\frac{v_F\Lambda}{M}\right)^2\right)} \tag{2.23}$$

2.4.1 Energy Bound States

In order to compute the energy levels of the bound states, we introduce an alternative version to the already defined integral equation for single impurity:

$$\begin{aligned} &\det\left(1 - \hat{H}^{Imp}\mathcal{G}_0^+(0;E)\right) = 0 \\ &\Rightarrow \det\begin{pmatrix} 1+\beta^+\mathcal{G}_0^{11+}(0;E) & 0 \\ 0 & 1+\beta^-\mathcal{G}_0^{22+}(0;E) \end{pmatrix} = 0 \end{aligned}$$

where we have used the notation $\beta^{\pm} = \dfrac{V_0 \pm V_3}{4\pi}$. Indeed, if we think of the integral equation as an eigenvalue equation for eigenvalue 1 and eigenvectors $(1,0)^{\dagger}, (0,1)^{\dagger}$, that determinant is perfectly understood. Compare with Balents [17].
We have to find the conditions that make the determinant vanish. First, we study the Green's function trends: they are respectively diverging at $|M|$ i.e. diverging at the edges of the system which we set as boundary, see plot.
Hence, the determinant is solved if we use the correct sign of both the impurity strength and the matrix elements of $\mathcal{G}_0^+(0;E)$ - since they are dependent. The energy values corresponding to bound states - which make the determinant vanish - are indeed those solving at least one of the equations of the system:

$$\begin{cases} 1 + \dfrac{V_0+V_3}{4\pi}\mathcal{G}_0^{11+}(0;E) = 0 & \Leftrightarrow \mathcal{G}_0^{11+}(0;E) < 0 \quad \Rightarrow \dfrac{V_0+V_3}{4\pi} < 0 \\ 1 + \dfrac{V_0-V_3}{4\pi}\mathcal{G}_0^{22+}(0;) = 0 & \Leftrightarrow \mathcal{G}_0^{22+}(0;E) > 0 \quad \Rightarrow \dfrac{V_0-V_3}{4\pi} > 0 \end{cases}.$$

where $\mathcal{G}_0^{11+}(0;E), \mathcal{G}_0^{22+}(0;E)$ are definite negative and positive, respectively. The energies bound states are given by the intersection between the curves of those matrix elements and the impurity strength. Before computing the energy bound state expressions, we can make a classification, as we can see from the plot:

- $V_3 = 0$ and any non-zero values of the scalar V_0 impurity. The strength will always intersect one of Green's function curves, hence we will find always at least one bound state

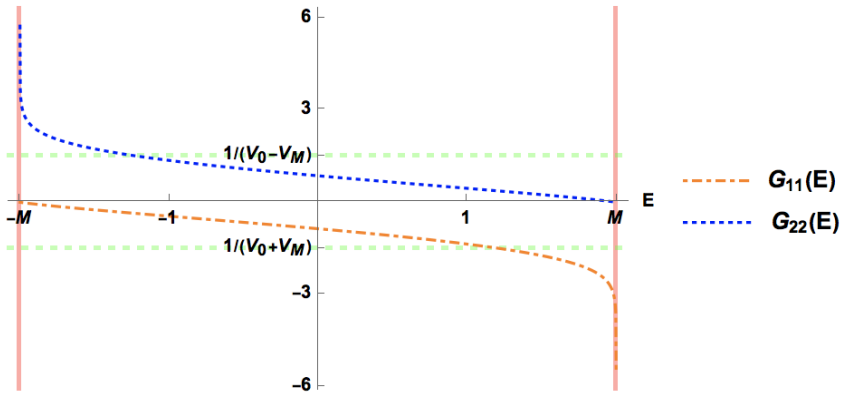

Figure 2.3: The Green's functions are diverging as they approach the edge states. The horizontal lines indicate the impurity strength. At an intersection among curves, the corresponding energy value indicates the energy of a bound state.

- $V_0 = 0$ and positive values of the magnetic V_3 impurity, there is no intersection at all between the impurity strength and the Green's functions, meaning there is no bound states. For $V_3 = 0$ and negative values of V_3, the impurity strength line will always intersect both Green's function curves, leading to two bound states - that we calculate next
- $\forall V_3, \forall V_0 \neq 0$ there are intermediate combinations of impurity strength. The general requirement to obtain two bound states in the system is $|V_0| < |V_3|$ with $V_3 < 0$

For our interest, we will consider only the case with magnetic impurity $V_3 < 0$ setting the scalar strength to zero.
So far we have imposed a condition over the impurity strength in order to match the Green's functions trends and to derive the bound states expression. Hence, the equation system we need to solve reads:

$$\begin{cases} 1 + \frac{V_3}{4\pi}(E+M)\log\left(1+\left(\frac{v_F\Lambda}{M}\right)^2\right) = 0 \\ 1 - \frac{V_3}{4\pi}(E-M)\log\left(1+\left(\frac{v_F\Lambda}{M}\right)^2\right) = 0 \end{cases},$$

where we think of those equations as eigenvalues equations for bound states energies with eigenvalue $\lambda_1 \equiv \lambda_2 = 1$ and eigenvectors:

$$\psi(0) = \begin{pmatrix} \psi_1(0) \\ \psi_2(0) \end{pmatrix}$$
$$\text{with } \psi_1(0) = \begin{pmatrix} 1 \\ 0 \end{pmatrix}, \psi_2(0) = \begin{pmatrix} 0 \\ 1 \end{pmatrix}.$$

The system of equations is solved for the following cases.
First case $E = 0$: we can immediately get condition on the strength of the impurity - indeed fully determined by the parameters we can easily tune:

$$\pm V_3 = \frac{\mp 4\pi}{M\log(1+(v_F\Lambda/M)^2)}.$$

Second case $E \neq 0$:

$$\begin{cases} E\frac{V_3}{4\pi}\log\left(1+\left(\frac{v_F\Lambda}{M}\right)^2\right) + M\frac{V_3}{4\pi}\log\left(1+\left(\frac{v_F\Lambda}{M}\right)^2\right) + 1 = 0 \\ E\frac{-V_3}{4\pi}\log\left(1+\left(\frac{v_F\Lambda}{M}\right)^2\right) + M\frac{V_3}{4\pi}\log\left(1+\left(\frac{v_F\Lambda}{M}\right)^2\right) + 1 = 0 \end{cases}$$

which are respectively solved for

$$E_{BS}^{\pm} = \mp\left[M + \frac{1}{\frac{V_3}{4\pi}\log\left(1+\left(\frac{v_F\Lambda}{M}\right)^2\right)}\right] \tag{2.24}$$

We note such expressions can be numerically evaluated either for a desired choice of parameters Λ, M or for required energy values in order to satisfy both cut-off and gap energy in the system. This is an important conclusion: we have derived an analitycal expression for energy levels corresponding to bound states due to the presence of one impurity at the center of the surface of 3D TI. Moreover, now we know that each bound state has either the trivial case $E = 0$ corresponding to the ground state or two discrete energy levels. We will use these energy expressions to derive the wave function related to such states. Once we start building the lattice of impurity - as we study in the next section - these levels will be dispersive and involved into band structure formation.

2.5 Lattice of Impurity Model

The actual model we want to study is composed by multiple impurities arranged in a rarefied isotropic 2D square lattice. We picture this condition as if we had grouped many independent single impurity with reciprocal distance given by lattice constant a_{Imp}. However, they are close enough to interact.

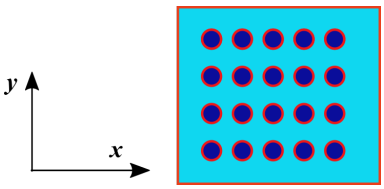

Figure 2.4: Sketch of impurity lattice setting.

Important to mention the distances we deal now are related to the sublattice of impurity, hence their corresponding wave functions belong to that sub-space.
The local bare propagator in real space is given by:

$$\mathcal{G}_0^+(\mathbf{r}=\mathbf{r}_j-\mathbf{r}_i;E) \equiv \mathcal{G}_0^+(\mathbf{r};E) = \int \frac{d^2\mathbf{k}}{(2\pi)^2}\mathcal{G}_0^+(\mathbf{k};E)e^{-i\mathbf{k}\cdot\mathbf{r}}.$$

The matrix form of the Green's function:

$$\mathcal{G}_0^+(\mathbf{r}=\mathbf{r}_j-\mathbf{r}_i;E) = \begin{pmatrix} X_0(|\mathbf{r}|)+X_1(|\mathbf{r}|) & X_2^+(|\mathbf{r}|) \\ X_2^-(|\mathbf{r}|) & X_0(|\mathbf{r}|)-X_1(|\mathbf{r}|)\end{pmatrix}$$

where the elements - recalling $\mathcal{G}_0^+(\mathbf{k};E)$ in eq.(2.22) - are defined as:

$$X_0(\mathbf{r})\mathbb{1} = (E\mathbb{1})\int_0^\Lambda \frac{d^2\mathbf{k}}{(2\pi)^2}\frac{e^{-i\mathbf{k}\cdot\mathbf{r}}}{E^2-M^2-v_F^2|\mathbf{k}|^2}$$

$$X_1(\mathbf{r})\tau_3 = (M\tau_3)\int_0^\Lambda \frac{d^2\mathbf{k}}{(2\pi)^2}\frac{e^{-i\mathbf{k}\cdot\mathbf{r}}}{E^2-M^2-v_F^2|\mathbf{k}|^2}$$

$$X_2^\pm(\mathbf{r})(\tau_1+\tau_2) = \int_0^\Lambda \frac{d^2\mathbf{k}}{(2\pi)^2}\frac{k_x \pm ik_y}{E^2-M^2-v_F^2|\mathbf{k}|^2}e^{-i\mathbf{k}\cdot\mathbf{r}}.$$

The calculation of the integrals involves K(z) - Second Kind Modified Bessel function of order 0 and 1: further details are shown in Appendix (C). Here, we present directly the resulting **Green's function lattice of impurity**:

$$\boxed{\mathcal{G}_0^+(\mathbf{r};E) = -\frac{1}{2\pi}\begin{pmatrix} (E+M)K_0\left(\frac{|\mathbf{r}|}{\xi}\right) & -i\frac{v_F}{\xi}e^{i\theta_r}K_1\left(\frac{|\mathbf{r}|}{\xi}\right) \\ -i\frac{v_F}{\xi}e^{-i\theta_r}K_1\left(\frac{|\mathbf{r}|}{\xi}\right) & (E-M)K_0\left(\frac{|\mathbf{r}|}{\xi}\right)\end{pmatrix}}. \tag{2.25}$$

where

$$e^{\pm i\theta_r} = \frac{r^x \pm ir^y}{\sqrt{(r^x)^2+(r^y)^2}} = \frac{r^x \pm ir^y}{|r|}$$

and ξ stands for the **correlation function** we compute below. The energy at the level of the Green's function fulfills the range $E < |M| \ll v_F\Lambda$ for negative magnetic impurity strength.

The correlation length

In the whole model we have set an energy range. We still have to compute a length scale: it is a useful parameter to compare distances where the coupling among impurities is active. Hence, we need to introduce the **correlation length** of the system.
According to the fact we have designed the impurity array as isotropic, the correlation length we calculate in 1D is the same in a 2D system.
Thus, we start with the retarded Green's function in 1D:

$$G_0^+(x;E) = \int \frac{dk}{2\pi}\frac{e^{ikx}}{E^2-M^2-v_F^2k^2}$$

and it has two poles on the real axis $k = \pm\sqrt{M^2-E^2}/v_F$.
We study the integral by means of the complex plane and we assume $x > 0$. Hence, the integral will converge only in the upper half-imaginary plane. According to the usual path of retarded propagator, only the positive pole will be enclosed into such a contour and so it is the only one evaluated though the Residue Theorem. The final result reads:

$$G_0^+(x;E) = \frac{1}{2\sqrt{M^2-E^2}/v_F}exp\Big(\frac{\sqrt{M^2-E^2}}{v_F}x\Big),$$

from that we define the correlation length

$$\boxed{\xi = \frac{v_F}{\sqrt{M^2-E^2}}}. \tag{2.26}$$

Asymptotic trend of matrix elements Green's function

The asymptotic behaviour of $\mathcal{G}_0^+(\mathbf{r};E)$ is computed again in Appendix (C).
We physically understand those trends in terms of hybridization of adjacent impurity sites. For small argument i.e. $|\mathbf{r}| \ll \xi$, the Green's function is slowly decaying, hence it is logarithmic diverging. For large argument i.e. $|\mathbf{r}| \gg \xi$, it is exponentially decaying - see plot below.
Since we allow long-range coupling among impurity sites, meaning we take into account hopping distances bigger than the correlation length, the exponantial decay is the suitable regime.
Moreover, we note after $5\xi/a_{Imp}$ the Green's function vanishes. We will use such a value as cut-off in the hopping process to evaluate any numerical calculation in the following.

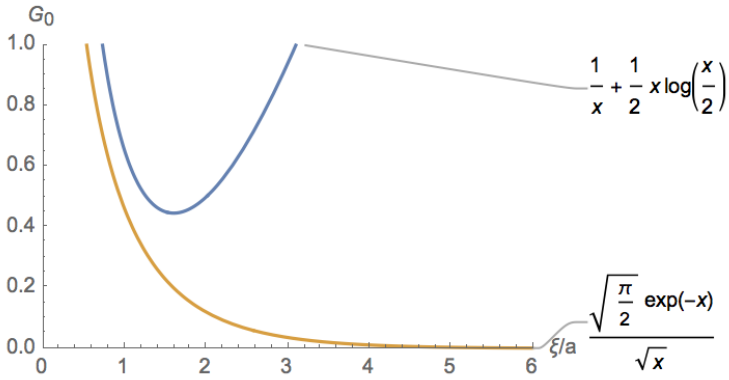

Figure 2.5: Green's function asymptotic trends in terms of correlation length over lattice impurity constant.

Wave function of Bound States

We have treated so far an in-gap two-band structure due to the lattice of the impurity. The global wave function of the bound states can be now derived.
We start considering the integral equation given in eq.(2.21), in terms of explicit distances:

$$\psi(\mathbf{r}=\mathbf{r}_j-\mathbf{r}_i)=\hat{H}^{Imp}\mathcal{G}_0^+(\mathbf{r}_j-\mathbf{r}_i;E)\psi(\mathbf{r}_j-\mathbf{r}_i)\quad\Longleftrightarrow\quad\Big(\mathbb{1}-\hat{H}^{Imp}\mathcal{G}_0^+(\mathbf{r}_j-\mathbf{r}_i;E)\Big)\psi(\mathbf{r}_j-\mathbf{r}_i)=0.$$

We implement the expression for the local bare propagator for multiple impurity $\mathcal{G}_0^+(\mathbf{r};E)$ derived in eq.(2.25), using its exponential expansion. And we plug into the Green's function the discrete energy levels defined in eq.(2.24) - since the case $E=0$ is trivial. Thus:

$$\psi(\mathbf{r})=\hat{H}^{Imp}\mathcal{G}_0^+(\mathbf{r};E_{BS}^{\pm})\psi(0)=\begin{pmatrix}\psi_1(\mathbf{r})\\ \psi_2(\mathbf{r})\end{pmatrix}$$

with

$$\psi_1(\mathbf{r})=\begin{pmatrix}(+V_3)\mathcal{G}_0^{11}(\mathbf{r};E_{BS}^+)\\ (-V_3)\mathcal{G}_0^{21}(\mathbf{r};E_{BS}^-)\end{pmatrix}\quad,\quad\psi_2(\mathbf{r})=\begin{pmatrix}(+V_3)\mathcal{G}_0^{12}(\mathbf{r};E_{BS}^+)\\ (-V_3)\mathcal{G}_0^{22}(\mathbf{r};E_{BS}^-)\end{pmatrix}$$

and eigenvectors

$$\psi(0)=\begin{pmatrix}\psi_1(\mathbf{r})\\ \psi_2(\mathbf{r})\end{pmatrix}$$
$$\text{with }\psi_1(\mathbf{r})=\begin{pmatrix}1\\0\end{pmatrix}\text{ , }\psi_2(\mathbf{r})=\begin{pmatrix}0\\1\end{pmatrix}.$$

Thus, the wave function $\psi(\mathbf{r})$ is evaluated for energy of bounds states at the impurity site. As outcome, the global wave function is made up by the convolution of the overlapped wave functions on neighboring impurity sites.

2.6 From the Exact Solution to the Effective Model

The main results from the previous paragraphs is the Green's function for a lattice of magnetic impurity, see eq.(2.25), and plugging it into eq.(2.21) we obtain:

$$\psi(\mathbf{r}_i)=V_M\tau_z\sum_{\mathbf{r}_j}\mathcal{G}_0^+(\mathbf{r}=\mathbf{r}_j-\mathbf{r}_i;E)\psi(\mathbf{r}_j).\tag{2.27}$$

We can re-arrange the summation in order to obtain an explicit form for both unique and multiple impurity case, that is splitting the equation into:

$$\psi(\mathbf{r}_i)=V_M\tau_z\mathcal{G}_0^+(0;E)\psi(\mathbf{r}_i)+V_M\tau_z\sum_{\mathbf{r}_j\neq\mathbf{r}_i}\mathcal{G}_0^+(\mathbf{r}_j-\mathbf{r}_i;E)\psi(\mathbf{r}_j),\tag{2.28}$$

and considering the case of one impurity at origin of lattice we conclude

$$\Big(\mathbb{1} - V_M\tau_z\mathcal{G}_0^+(0;E)\Big)\psi(0) = V_M\tau_z\sum_{\mathbf{r}_j\neq\mathbf{r}_i}\mathcal{G}_0^+(\mathbf{r}_j-\mathbf{r}_i;E)\psi(\mathbf{r}_j). \tag{2.29}$$

We note the left-hand-side is identified by the local propagator for one impurity, see eq.(2.23). On the right-hand-side we find the propagator for multiple impurity, see eq.(2.25).
This equation is an exact solution, meaning that we have found a *self-consistent equation* we have to solve by iteration. This is not an affordable problem, especially for the computationally point of view. Moreover, that exact equation isn't equivalent to the original Schödinger equation. We need to introduce some approximations in order to reconnect our result to an effective model.
We consider as a good approximation to set the energies of the Green's function equal to the energies of the in-gap bound states themselves. The collection of those emerging bound states will create band structure. However, because of the lattice constant $a_{Imp} \gg a_{Bulk}$, the overlap among neighboring impurity is weak i.e. we are under weak hybridization conditions. Thus, we can reasonably approximate - at the level of the Green's function - the energies of the in-gap bound states to be very tiny, eventually equal to zero. According to the energy scale of the system, we think of $E_{BS}^{\pm}/|M| = [10^{-1};10^{-2}]$. Indeed, the requirement to set the energy bound states very in the center of the gap is necessary not only to avoid any connections with the edge states but also to assume such an approximation, i.e. **diluite condition**. The interested range of energies is mainly confined into the center of the gap.
Therefore, the exact solution becomes an effective integral equation and it is indeed equivalent to the original Schrödinger equation. From that we can read off the effective Hamiltonian.
We start now making use of the approximations. We expand around $E \sim E_{BS}^{\pm} \simeq 0$ up to the first order the equation (2.28):

$$\begin{aligned}&\Big(\mathbb{1} - V_M\tau_z\big(\mathcal{G}_0^+(0;0) + E_{BS}^{\pm}\partial_{E_{BS}^{\pm}}\mathcal{G}_0^+(0;E_{BS}^{\pm})\big|_{E_{BS}^{\pm}=0}\big)\Big)\psi(0)\\ &= V_M\tau_z\sum_{\mathbf{r}_j\neq\mathbf{r}_i}\Big(\mathcal{G}_0^+(\mathbf{r};0) + E_{BS}^{\pm}\partial_{E_{BS}^{\pm}}\mathcal{G}_0^+(\mathbf{r};E_{BS}^{\pm})\big|_{E_{BS}^{\pm}=0}\Big)\psi(\mathbf{r}_j)\end{aligned} \tag{2.30}$$

and we can neglect the linear term in energy of the Green's function depending on the distance in comparison to the one impurity case, hence $E_{BS}^{\pm}\partial_{E_{BS}^{\pm}}\mathcal{G}_0^+(\mathbf{r};E_{BS}^{\pm}) \sim 0$.
The final version of the effective-integral equation reads

$$\Big(\mathbb{1} - V_M\tau_z\mathcal{G}_0^+(0;0)\Big)\psi(0) = V_M\tau_z\sum_{\mathbf{r}_j\neq\mathbf{r}_i}\mathcal{G}_0^+(\mathbf{r};0)\psi(\mathbf{r}_j) \tag{2.31}$$

that is in explicit terms:

$$\begin{aligned}&\Big(\mathbb{1} + V_M\tau_z\big(\frac{E\mathbb{1}+M\tau_z}{4\pi}\big)\log\big(1+\big(\frac{v_F\Lambda}{M}\big)^2\big)\Big)\psi(0) =\\ &V_M\tau_z\big(\frac{-1}{2\pi}\big)\sum_{\mathbf{r}_j\neq\mathbf{r}_i}\Big(M\tau_z K_0\Big(\frac{|\mathbf{r}_j-\mathbf{r}_i|}{\xi_0}\Big) - i\frac{v_F}{\xi_0}\frac{r^x\tau_x - r^y\tau_y}{\sqrt{(r^x)^2+(r^y)^2}}K_1\Big(\frac{|\mathbf{r}_j-\mathbf{r}_i|}{\xi_0}\Big)\Big)\psi(\mathbf{r}_j)\end{aligned} \tag{2.32}$$

where $\xi_0 = v_F/M$.
At this stage, we have an **integral-effective equation equivalent** to the original Schrödinger equation. Now, we have to manipulate it in order to extract an expression for the effective Hamiltonian of the model.
We start with:

$$E\psi(\mathbf{r}_i) = \sum_{\mathbf{r}_j} H_{ij}\psi(\mathbf{r}_j),$$

and we have to isolate in eq.(2.32) all terms liner in energy on the left side and all the rest on the right hand side - where we can read finally the Hamiltonian. Looking at the left hand

side of integral equation (2.32), it is easily cast just isolating the energy term from the rest, dividing both side of the equation for $(\frac{V_M}{4\pi}\log(1+(\frac{v_F\Lambda}{M})^2))^{-1}$. Whereas, the right hand side needs some further notation, useful for the next chapter too. We start defining:

$$\frac{r^x\tau_x - r^y\tau_y}{\sqrt{(r^x)^2+(r^y)^2}} = \frac{r^x}{|r|}\tau_x - \frac{r^y}{|r|}\tau_y = \Re\Delta_r\tau_x - \Im\Delta_r\tau_y.$$

Then,

$$\begin{aligned}\sum_{\mathbf{r}_j\neq\mathbf{r}_i} M\tau_z \underbrace{K_0\left(\frac{|\mathbf{r}_j-\mathbf{r}_i|}{\xi_0}\right)}_{h_{\mathbf{r}_j-\mathbf{r}_i}} - i\frac{v_F}{\xi_0}\left(\Re\Delta_r\tau_x - \Im\Delta_r\tau_y\right)\underbrace{K_1\left(\frac{|\mathbf{r}_j-\mathbf{r}_i|}{\xi_0}\right)}_{\Delta_{\mathbf{r}_j-\mathbf{r}_i}} \\ = \sum_{\mathbf{r}}\begin{pmatrix} Mh_{\mathbf{r}} & \frac{v_F}{\xi_0}\Delta_r\Delta_{\mathbf{r}} \\ \frac{v_F}{\xi_0}\Delta^\star_{-r}\Delta_{\mathbf{r}} & -Mh_{\mathbf{r}}\end{pmatrix}\end{aligned} \tag{2.33}$$

where $|\mathbf{r}_j-\mathbf{r}_i|=\mathbf{r}$.
Once those manipulations are completed, the final **effective equation** reads:

$$\begin{aligned}E\psi(\mathbf{r}_i) &= \sum_{\mathbf{r}_j} H_{ij}\psi(\mathbf{r}_j) \\ &= -\left[\left(\frac{V3}{4\pi}\log(1+(\frac{v_F\Lambda}{M})^2\right)^{-1} + M\right]\tau_z\psi(\mathbf{r}_j)\delta_{\mathbf{r}_j,\mathbf{r}_i} \\ &- \frac{4}{\log\left(1+(\frac{v_F\Lambda}{M})^2\right)}\sum_{\mathbf{r}_j\neq\mathbf{r}_i}\left[Mh_{\mathbf{r}_j-\mathbf{r}_i}\tau_z - i\frac{v_F}{\xi_0}\left(\Re\Delta_r\tau_x - \Im\Delta_r\tau_y\right)\Delta_{\mathbf{r}_j-\mathbf{r}_i}\right]\psi(\mathbf{r}_j) \\ &= E^+_{BS}\tau_z\psi(\mathbf{r}_j)\delta_{\mathbf{r}_j,\mathbf{r}_i} - \frac{4}{\log\left(1+(\frac{v_F\Lambda}{M})^2\right)}\sum_{\mathbf{r}_j\neq\mathbf{r}_i}\mathcal{G}^+_0(\mathbf{r}_j-\mathbf{r}_i;0)\psi(\mathbf{r}_j)\end{aligned} \tag{2.34}$$

where E^+_{BS} can be regarded as the *effective-mass* of the model.
Making more explicit the results we have found, we show the two cases.
If $\mathbf{r}_j=\mathbf{r}_i=0$, thus we regard the surface with one impurity at its origin:

$$\begin{aligned}&E\psi(0) = -\left[\left(\frac{V3}{4\pi}\log(1+(\frac{v_F\Lambda}{M})^2\right)^{-1} + M\right]\tau_z\psi(0) \\ &\Rightarrow \boxed{H_{ii} = -\begin{pmatrix}\left(\frac{V3}{4\pi}\log(1+(\frac{v_F\Lambda}{M})^2\right)^{-1} + M & 0 \\ 0 & -\left(\frac{V3}{4\pi}\log(1+(\frac{v_F\Lambda}{M})^2\right)^{-1} - M\end{pmatrix}}\end{aligned} \tag{2.35}$$

If $\mathbf{r}_j\neq\mathbf{r}_i, \mathbf{r}_i\neq 0$, thus we regard the surface with a square lattice of impurity:

$$\begin{aligned}E\psi(\mathbf{r}_i) &= \underbrace{-\frac{4}{\log\left(1+(\frac{v_F\Lambda}{M})^2\right)}}_{\gamma}\sum_{\mathbf{r}_j\neq\mathbf{r}_i}\begin{pmatrix} Mh_{\mathbf{r}_j-\mathbf{r}_i} & -i\frac{v_F}{\xi_0}\frac{r^x+ir^y}{|r|}\Delta_{\mathbf{r}_j-\mathbf{r}_i} \\ -i\frac{v_F}{\xi_0}\frac{r^x-ir^y}{|r|}\Delta_{\mathbf{r}_j-\mathbf{r}_i} & -Mh_{\mathbf{r}_j-\mathbf{r}_i}\end{pmatrix}\psi(\mathbf{r}_j) \\ &\Rightarrow \boxed{H_{ij} = -\frac{4}{\log\left(1+(\frac{v_F\Lambda}{M})^2\right)}\sum_{\mathbf{r}_j\neq\mathbf{r}_i}\begin{pmatrix} Mh_{\mathbf{r}_j-\mathbf{r}_i} & -i\frac{v_F}{\xi_0}\frac{r^x+ir^y}{|r|}\Delta_{\mathbf{r}_j-\mathbf{r}_i} \\ -i\frac{v_F}{\xi_0}\frac{r^x-ir^y}{|r|}\Delta_{\mathbf{r}_j-\mathbf{r}_i} & -Mh_{\mathbf{r}_j-\mathbf{r}_i}\end{pmatrix}}.\end{aligned} \tag{2.36}$$

As conclusion of the chapter, we have derived the **effective two-band Hamiltonian** in equation (2.34) of the model in real space for both cases on the surface of the 3D strong TI. That can be summarized in the matrix structure of the effective Hamiltonian

$$\hat{H}_{ij} = \begin{pmatrix} h_{\mathbf{r}_{ij}} & \Delta_{\mathbf{r}_{ij}} \\ \Delta^{\star}_{\mathbf{r}_{ij}} & -h_{\mathbf{r}_{ij}} \end{pmatrix} \tag{2.37}$$

where

$$h_{\mathbf{r}_{ij}} = \begin{cases} E^{+}_{BS} \quad , \quad \mathbf{r}_i = \mathbf{r}_j = 0 \\ \gamma M K_0\left(\dfrac{|\mathbf{r}_j - \mathbf{r}_i|}{\xi_0}\right) \quad , \quad \mathbf{r}_i \neq \mathbf{r}_j \end{cases}$$

$$\Delta_{\mathbf{r}_{ij}} = \begin{cases} 0 \quad , \quad \mathbf{r}_i = \mathbf{r}_j = 0 \\ -\gamma \dfrac{i v_F}{\xi_0} \dfrac{r^x + i r^y}{|r|} K_1\left(\dfrac{|\mathbf{r}_j - \mathbf{r}_i|}{\xi_0}\right) \quad , \quad \mathbf{r}_i \neq \mathbf{r}_j \end{cases} .$$

Chapter 3

Features of the Model and its Chern Numbers

As main result of the previous chapter is the two-band effective Hamiltonian of a discrete lattice system in real space, see eq.(2.34). The bands are described by Tight-Binding approximation - at least within the First Brillouoin Zone. Once that Hamiltonian is turned into momentum space, that is the Dirac Hamiltonian, we have all the elements to analyse its energy spectrum. Then, we can calculate the topological invariant property of the gapped-bands i.e. the Chern Numbers, giving both numerical and skyrmionic results.
According to the outcome we will be able to finally describe the model response.

3.1 Towards the Dirac Equation

In order to evaluate the Chern Numbers of the in-gap band structure created by the square array of impurity and study its energy spectrum, we need a suitable form of the effective Hamiltonian in momentum space.
Since we have a two-band model, that is achieved by turning it into a Dirac Equation. After performing the 2D Fourier Transform, the Hamiltonian is a complex $2x2$ matrix whose bases are formed by the Pauli matrices and the unit matrix. Since we have a lattice model with lattice constant a, the summation in eq.(2.34) over any $\mathbf{r}_j \neq \mathbf{r}_i$ is replaced by its discrete 2D-coordinates version. Similarly, in Δ_r the term r_x, r_y are written for the same 2D lattice coordinates. Hence, the used 2D vectors read:

$$\mathbf{r}_i = a \begin{pmatrix} n \\ m \end{pmatrix} \quad \mathbf{r}_j = a \begin{pmatrix} n' \\ m' \end{pmatrix} \quad ,$$

in particular, we have a square lattice, so we can write

$$|\mathbf{r}_j - \mathbf{r}_i| = |\mathbf{r}| = a\sqrt{n^2 + m^2}.$$

We present the definition of the 2D Fourier Transform for the effective Hamiltonian:

$$H_{\mathbf{k}} = \sum_{\mathbf{r}} e^{i\mathbf{k}\cdot\mathbf{r}} H(\mathbf{r}) = \sum_{\mathbf{r}_x,\mathbf{r}_y} e^{i(\mathbf{k}_x\cdot\mathbf{r}_x + \mathbf{k}_y\cdot\mathbf{r}_y)} H(\mathbf{r}_x, \mathbf{r}_y) \tag{3.1}$$

where summation runs over each lattice sites - over both the axes and the four quadrants - taking into account long-range hopping among all impurity sites. Compare this expression with the introductory study in Appendix (B) concerning a 2D Fourier Transform on the x, y-axes only.

We introduce some further notation in the matrix elements of the effective Hamiltonian

$$H(\mathbf{r}) = \sum_{\mathbf{r}} \begin{pmatrix} Mh_{\mathbf{r}} & \frac{v_F}{\xi_0}\overbrace{\Delta_r\Delta_{\mathbf{r}}}^{\overline{\Delta_{\mathbf{r}}}} \\ \frac{v_F}{\xi_0}\underbrace{\Delta^\star_{-r}\Delta_{\mathbf{r}}}_{\overline{\Delta^\star_{-\mathbf{r}}}} & -Mh_{\mathbf{r}} \end{pmatrix},$$

to clearly define the Fourier Transform of each element:

$$\begin{aligned} H_{\mathbf{k}} &= \sum_{\mathbf{r}} e^{i\mathbf{k}\cdot\mathbf{r}} H(\mathbf{r}) \\ &= \begin{pmatrix} M\sum_{\mathbf{r}} e^{i\mathbf{k}\cdot\mathbf{r}} h_{\mathbf{r}} & \frac{v_F}{\xi_0}\sum_{\mathbf{r}} e^{i\mathbf{k}\cdot\mathbf{r}}\overline{\Delta_{\mathbf{r}}} \\ \frac{v_F}{\xi_0}\sum_{\mathbf{r}}\left(e^{-i\mathbf{k}\cdot\mathbf{r}}\overline{\Delta_{-\mathbf{r}}}\right)^\star & -M\sum_{\mathbf{r}} e^{i\mathbf{k}\cdot\mathbf{r}} h_{\mathbf{r}} \end{pmatrix} \\ &= \begin{pmatrix} Mh_{\mathbf{k}} & \frac{v_F}{\xi_0}\overline{\Delta_{\mathbf{k}}} \\ \frac{v_F}{\xi_0}\overline{\Delta^\star_{\mathbf{k}}} & -Mh_{\mathbf{k}} \end{pmatrix} = \begin{pmatrix} Mh_{\mathbf{k}} & \frac{v_F}{\xi_0}\left(\Re(\overline{\Delta_{\mathbf{k}}}) + i\Im(\overline{\Delta_{\mathbf{k}}})\right) \\ \frac{v_F}{\xi_0}\left(\Re(\overline{\Delta_{\mathbf{k}}}) - i\Im(\overline{\Delta_{\mathbf{k}}})\right) & -Mh_{\mathbf{k}} \end{pmatrix} \\ &= \Re(\overline{\Delta_{\mathbf{k}}})\cdot\tau_x + \Im(\overline{\Delta_{\mathbf{k}}})\cdot\tau_y + h_{\mathbf{k}}\cdot\tau_z \end{aligned} \tag{3.2}$$

where we observe the off-diagonal terms have both real and imaginary part recalling that $\Delta_r = \Re\Delta_r\tau_x - \Im\Delta_r\tau_y$, see the previous Chapter 2. In the final line we have arranged the matrix components proportional to the corresponding Pauli Matrices bases only - since we have a zero chemical potential. This line is the Dirac form of the Hamiltonian.
Now, we are ready to compute the elements. First, we start with diagonal ones:

$$\begin{aligned} h_{\mathbf{k}} &= \sum_{m,n=1}^{+\infty} h_{mn}\left(\frac{a\sqrt{n^2+m^2}}{\xi_0}\right)e^{ia(k_x n + k_y m)} \\ &= h_{00}(0) + \sum_{n=1}^{+\infty} h_{0,n}\left(\frac{a|n|}{\xi_0}\right)2\cos(ak_x n) + \sum_{m=1}^{+\infty} h_{m,0}\left(\frac{a|m|}{\xi_0}\right)2\cos(ak_y m) \\ &+ \sum_{m,n=1}^{+\infty} h_{mn}\left(\frac{a\sqrt{n^2+m^2}}{\xi_0}\right)4\cos(ak_x n)\cos(ak_y m) \end{aligned} \tag{3.3}$$

where the first term indicates the case of one impurity i.e. $\mathcal{G}_0^+(0; E=0)$ and the two middle terms can be grouped together since we have a square lattice. Filling in the corresponding functions, we get:

$$\begin{aligned} h_{\mathbf{k}} = E^+_{BS}\delta_{nm} - \frac{4}{\log\left(1+(\frac{v_F\Lambda}{M})^2\right)}M\Bigg(&\sum_{n=1}^{\mathcal{C}}\left(K_0\left(\frac{a|n|}{\xi_0}\right)2\cos(ak_x n) + K_0\left(\frac{a|n|}{\xi_0}\right)2\cos(ak_y n)\right) \\ &+ \sum_{m,n=1}^{\mathcal{C}} K_0\left(\frac{a\sqrt{n^2+m^2}}{\xi_0}\right)4\cos(ak_x n)\cos(ak_y m)\Bigg) \end{aligned} \tag{3.4}$$

where it has been introduced the numerical cut-off on the summation $\mathcal{C} = 5\xi/a$, as we mentioned in the asymptotic behaviour of the Green's function in Chapter 2. Recalling the real space matrix structure, this matrix element will be in the basis of τ_z - it is renamed as d_z.

Secondly, the off-diagonal elements:

$$\begin{aligned}\overline{\Delta_{\mathbf{k}}} &= \sum_{m,n=1}^{+\infty} \frac{a(n+im)}{a\sqrt{n^2+m^2}} \Delta_{mn}\left(\frac{a\sqrt{n^2+m^2}}{\xi_0}\right) e^{ia(k_x n + k_y m)} \\ &= \sum_{n=1}^{+\infty} \Delta_{0,n}\left(\frac{a|n|}{\xi_0}\right) 2\sin(ak_x n) + \sum_{m=1}^{+\infty} \Delta_{0,n}\left(\frac{a|m|}{\xi_0}\right) 2i\sin(ak_y m) \\ &+ \sum_{m,n=1}^{+\infty} \Delta_{m,n}\left(\frac{a\sqrt{n^2+m^2}}{\xi_0}\right) \frac{4}{\sqrt{n^2+m^2}} \Big(n\sin(ak_x n)\cos(ak_y m) + im\cos(ak_x n)\sin(ak_y m)\Big).\end{aligned} \tag{3.5}$$

We can split it into x-component, with its functions and cut-off:

$$\frac{-4}{\log\left(1+(\frac{v_F\Lambda}{M})^2\right)} \frac{v_F}{\xi_0}\left(\sum_{n=1}^{\mathcal{C}} K_1\left(\frac{a|n|}{\xi_0}\right) 2\sin(ak_x n) + \sum_{m,n=1}^{\mathcal{C}} K_1\left(\frac{a\sqrt{n^2+m^2}}{\xi_0}\right) \frac{4n\sin(ak_x n)\cos(ak_y m)}{\sqrt{n^2+m^2}}\right) \tag{3.6}$$

it will be in τ_x basis and it is renamed as d_x.
And last, the y-component into τ_y basis giving the d_y term:

$$\frac{-4}{\log\left(1+(\frac{v_F\Lambda}{M})^2\right)} \frac{v_F}{\xi_0}\left(\sum_{m=1}^{\mathcal{C}} K_1\left(\frac{a|m|}{\xi_0}\right) 2\sin(ak_y m) \sum_{m,n=1}^{\mathcal{C}} K_1\left(\frac{a\sqrt{n^2+m^2}}{\xi_0}\right) \frac{4m\cos(ak_x n)\sin(ak_y m)}{\sqrt{n^2+m^2}}\right). \tag{3.7}$$

We derived all the ingredients to write down the **Dirac Equation** in terms of the **d**-vectors we just found:

$$\boxed{H_{\mathbf{k}} = \mathbf{d}(\mathbf{k})\cdot\boldsymbol{\tau} = d_x(\mathbf{k})\tau_x + d_y(\mathbf{k})\tau_y + d_z(\mathbf{k})\tau_z}. \tag{3.8}$$

This *effective*-Dirac Hamiltonian can well represent the trend of the system in the vicinity of the critical points in the Brillouin zone. These points are the **k** values where the system undergoes into a non-adiabatic transformation i.e. the gap closes. In such a gapless system, the vectors $\mathbf{d}(\mathbf{k}_{crit}) = 0$ for $\mathbf{k}_{crit} = ((0,0),(\pi,0),(0,\pi),(-\pi,0),(0,-\pi)$, see scheme in fig.(3.1). Indeed, calculating the Chern Numbers at these $\mathbf{k}_{crit}$, its values change from ± 1 to 0 at gap closing. And the system enters in a trivial topological phase. Once the system passes again into another critical point, the gap opens and the Chern Numbers turns from 0 to ∓ 1 - hence we register a topological phase. Thus, any time we pass through a critical point the system changes phase. For any other values of **k** the system is always gapped with $\mathbf{d}(\mathbf{k}) \neq 0$ and the Chern Numbers shows a topological phase.

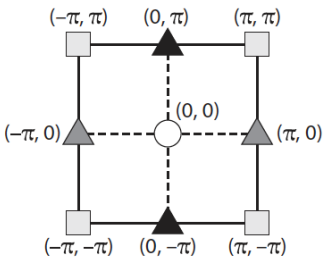

Figure 3.1: Scheme of the critical points (triangles) in the first Brillouin Zone, where the system becomes gapless. For any other values, the system is gapped, hence the calculation of the Chern Numbers for any other values is non-trivial. [10]

Hence, the Dirac equation is an ideal detector of Chern Numbers variation - as topological invariant property of non-trivial gapped band structure.

3.2 The energy spectrum

Up to this stage we have derived an effective Hamiltonian both in real space and its Dirac version for an impurity lattice on the surface of a strong 3D TI. This section will discuss the energetic aspects of the model, leading to a more complete understanding of the system itself.

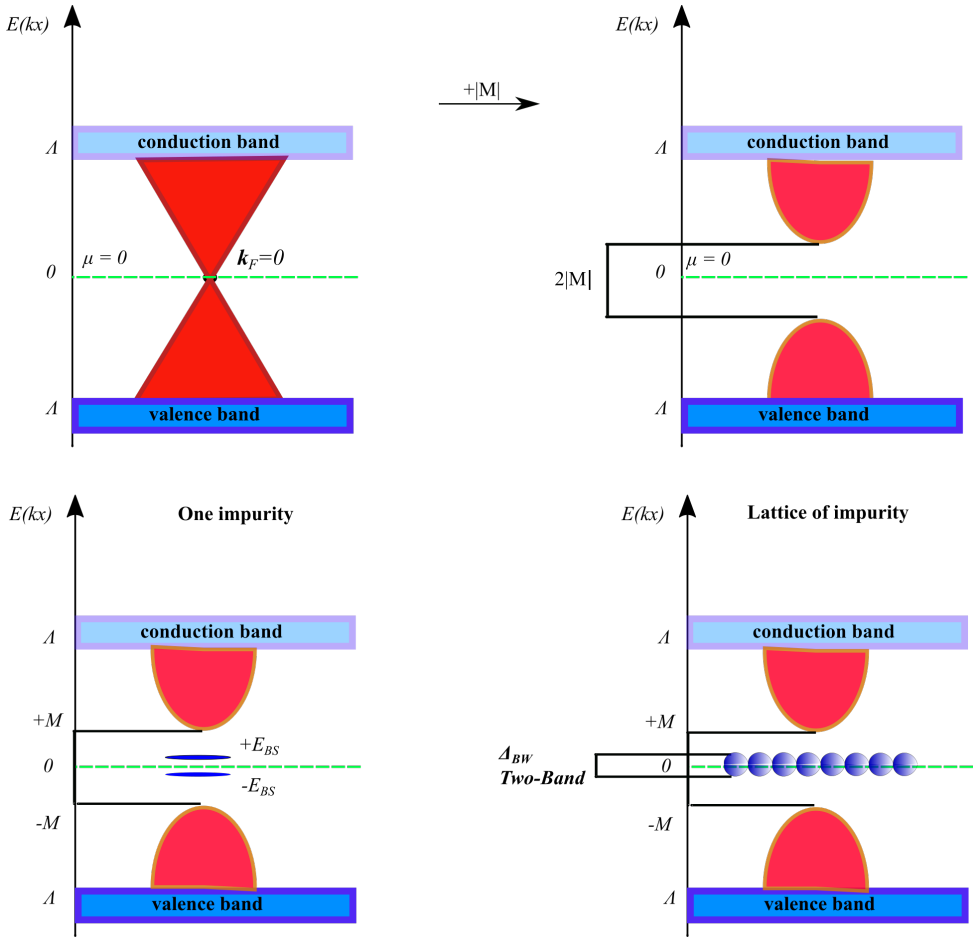

Figure 3.2: Sketch of energy spectrum model.

We start with a description of the model regarding modifications over the energy spectrum, see the scheme. The 3D TI works as basement of the setting, it can be regarded as the bulk and its valence and conduction bands are flat in comparison to the band structure we are going to create inside the gap. The "bare" system is the top surface, defined in $\hat{H}_{surface} = v_F(k_x\tau_x + k_y\tau_y)$. Its energy spectrum is represented by a unique *Dirac cone*, since the topological insulator is strong. And the extension of the surface energy dispersion is up to the momentum cut-off Λ that we set at the beginning of the Green's function matrix elements calculation. Hence, the cone is confined by the flat-band of the bulk. In such a configuration, we clearly see the bulk band structure plays no role in what is happening at the level of the Dirac point at $k_F = 0$. This specif is just an arbitrary choice. The bulk bandwidth can be then identified by $v_F \times \Lambda = D_{bulk}$.
We note the chemical potential, i.e. $\mu\mathbb{1}$, is set to zero and passes through the unique Dirac point.
Next, placing a ferromagnetic material close to that surface, we open a gap into the cone dispersion - so we break the time-reversal symmetry on the top surface. The mass term $+|M|\tau_z$ indicates that - the Hamiltonian turns into massive one. Edge states appear, they consist of propagating modes - meaning we have *chiral edge states*. If we eventually calculated the

wave functions of the edge, we would find the corresponding eigenstates as follow. For energy values on one channel, the wave function lives on one edge only - if we calculate it in the center of the gap - and then it delocalises if we are away from the center. Repeating the same calculation for the other channel, its eigenstate is located at the exact opposite edge: indeed, at the center of the gap, the two wave functions switch and then delocalise. If we compute the wave function for an eigenstaste on either valence or conduction bands, it turns out these states live into the bulk of the 3D TI.
Finally, we display an array of impurity which is defined by $\hat{H}_{imp}(\mathbf{r}) = \sum_i \overrightarrow{V} \cdot \overrightarrow{\tau}\delta(\mathbf{r} - \mathbf{r}_i)$. We tune their energy levels in order to have them within the gap - in the center of the gap, to avoid any interferences with the edges and to reasonably use the dilute approximation. These energies are in-gap bound states energies. The collection of impurity energies creates two-band structure with a corresponding bandwidth. Such non-trivial band structure is suitable to calculate the topological invariant integers value i.e. Chern Numbers.

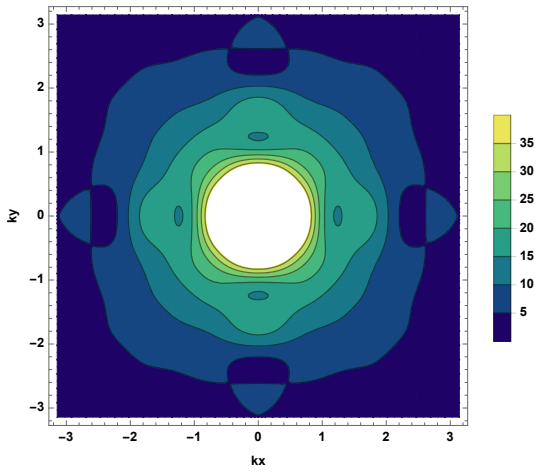

(a) $+E_{\mathbf{k}}$

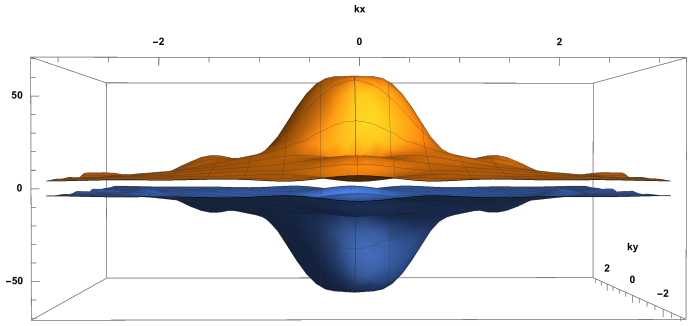

(b) $E_{\mathbf{k}}$

Figure 3.3: Recalling the structure of the effective equation in eq.(2.34), we take $\epsilon_0 = 0$ and mass term equal to 5. (a) Contour plot of the energy dispersion of the upper band $+E_{\mathbf{k}}$ as function of k_x, k_y in FBZ. (b) Plot of the energy dispersion.

Next, we introduce the energy dispersion the Dirac Hamiltonian, namely:

$$E_{\mathbf{k}} = \pm\sqrt{d_x(\mathbf{k})^2 + d_y(\mathbf{k})^2 + d_z(\mathbf{k})^2}. \tag{3.9}$$

The energy dispersion of upper band, i.e. the solution with positive sign, has a maximum at the center of the Brilloiun Zone and decreases towards the boundary. Indeed, taking both solutions, the energy dispersion is peaked at the origin, confront with the plots in fig.3.3.

3.3 The Chern Numbers

We are finally ready to study the topological property of system.
An important quantity we need is the *unit vector*, meaning the normalised version of the **d**-vectors previously found:

$$\widehat{\mathbf{d}}(\mathbf{k}) = \frac{\mathbf{d}(\mathbf{k})}{|\mathbf{d}(\mathbf{k})|}.$$

The array of magnetic impurity creates a band structure; on that we can calculate the integer-value topological invariant for time-reversal broken symmetry systems i.e. the **Chern Number**, with formula:

$$\boxed{C = \pm\frac{1}{2\pi}\int_{-\pi}^{\pi} dk_x \int_{-\pi}^{\pi} dk_y \frac{\mathbf{d}(\mathbf{k})}{2|\mathbf{d}(\mathbf{k})|} \cdot \left(\frac{\partial}{\partial k_x}\frac{\mathbf{d}(\mathbf{k})}{|\mathbf{d}(\mathbf{k})|} \times \frac{\partial}{\partial k_y}\frac{\mathbf{d}(\mathbf{k})}{|\mathbf{d}(\mathbf{k})|}\right)}. \tag{3.10}$$

We have numerically evaluated it up to $5(\xi/a_{Imp})$, cut-off chosen according to the exponential decay of the Green's function.
The result we have found is either *zero* - standing for trivial phase of the system - or *absolute value of 1* - a topological phase, see the trends in fig.(3.4).

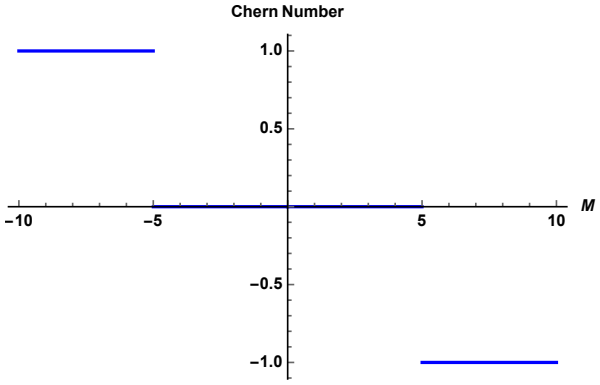

Figure 3.4: The plot shows the variation of the Chern Numbers with respect to the mass term values. These values have been derived through manipulation of the skyrmion number of the **d**-vectors. See later the skyrmionic configurations.

Thus, we conclude the surface of a 3D strong TopoIogical Insulator with the addition of a square array of magnetic impurity behaves like a **Chern insulator**.

A complementary view to support our numerical results is the study of the gap closing conditions by plotting the **d**-vectors - that maps the 2D Brilloiun Zone to the surface of a unit Bloch sphere.
We introduce a new concept. The winding number $\widehat{\mathbf{d}}$-vector integrated over the whole Brilloiun Zone is equivalent to the **skyrmion number** of the $\widehat{\mathbf{d}}$ itself. Recalling the map made by the **d**-vector, we can interpret the skyrmion number as follow.
If the direction of the vectors at the $(0,\pi), (\pi,0), (-\pi,0), (0,-\pi)$ - hence at the boundary of the BZ, see again scheme in fig.(3.1) - is anti-aligned to the vector in $(0,0)$, it means we are in a topological phase. That is geometrically interpreted as $\widehat{\mathbf{d}}$-vector enclosing the origin in the Bloch Sphere. If they are aligned, the $\widehat{\mathbf{d}}$-vector is wrapping on the sphere closed circles which don't enclose the origin. Thus, this is a trivial phase. These are the two possible configurations.
Tuning the unit vector, hence the values of ϵ_0, we have found the exact values of mass term M to realise gap closing transitions. For any value of the mass term smaller than -5 and bigger than 5, the system behaves like a Chern Insulator. In the intermediate range, the system is reduced to a trivial insulator. Results are shown below.

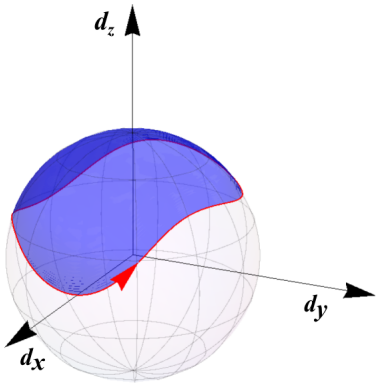

Figure 3.5: Geometric interpretation of the unit vector of the unit Bloch sphere. [9]

The skyrmion number plots remind *vortices*: we can think of those as corresponding $\mathbf{k}_{crit}$ values in the Brillouin Zone where the system becomes gapless.

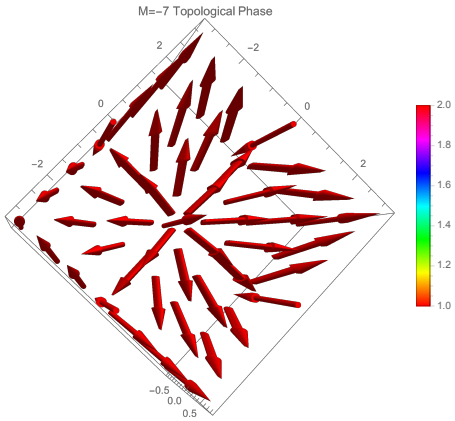

Figure 3.6: $M < -5$, *Topological*

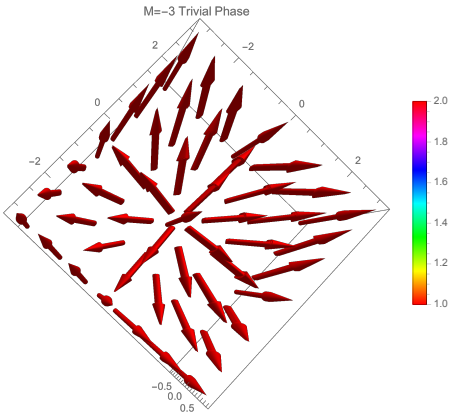

Figure 3.7: $-5 < M < 5$, *Trivial*

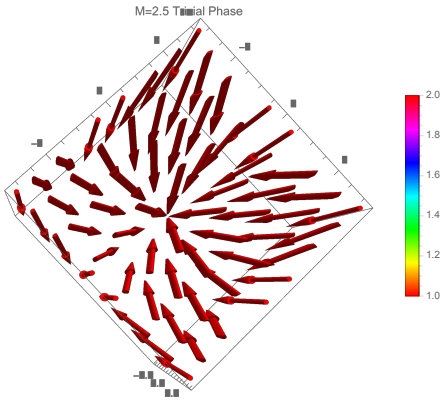

Figure 3.8: $-5 < M < 5$, *Trivial*

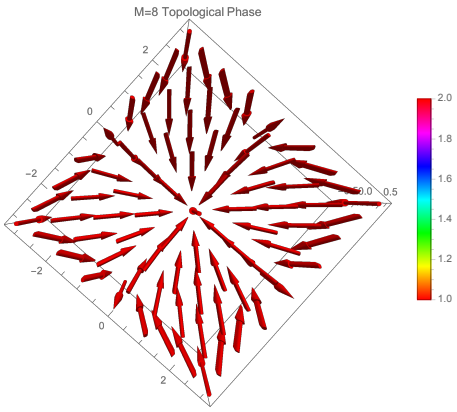

Figure 3.9: $M > 5$, *Topological*

Figure 3.10: Configurations of skyrmion number. Compare the mass values with the plot in fig.(3.4).

Chapter 4

Discussion and Outlook

The results we have achieved so far indicates that the top surface of the 3D strong Topological Insulator with a square lattice of magnetic impurity behaves like a **Chern Insulator**.
According to the fact we have placed an isotropic array of impurity and considered a long-range hopping with weak hybridization among all lattice sites, the configuration of any arbitrary lattice will not affect the result. Moreover, the impurity lattice restores the translational invariant in the top surface. Thus, we can safely conclude our outcome is a quite robust one.
Moreover, as already mentioned, our results can be experimentally verified. A simple setting we can think of is the semimetal 3D strain of $HgTe$ as bulk 3D Topological Insulator with an energy gap in the surface spectrum due to a ferromagnetic slab like iron - in the vicinity of the surface. The lattice of magnetic impurity can be achieved using iron. And we understood that our setting is responding as a Chern Insulator. From a practical perspective, the possibility to experimentally realise the model represents a competitive advantage compared to the p-wave superconductors since it can be experienced through available, expressly built, tested materials.

As final outlook of the project, some improvements are likely to be relevant in the setting.
A first insight is given by the band structure itself we have created. In the whole model we have designed the impurity with two initial discrete, non-degenerate energy levels hence we have two bound states in the system. And the resulting band structure is a two-band one. Increasing the number of bands implies not only doubling the initial impurity energy levels but increasing the unit size cell of the lattice itself. However, because we have just concluded the lattice configuration is arbitrary, this implementation might not affect much the result. And it might not lead to an increment of the Chern Numbers.
A more promising direction comes from comparing the energy spectrum initial conditions of our model to the reference paper [16].
In our model, the energy spectrum starts with a single Dirac cone - because we have a strong topological insulator - and the chemical potential is set to zero. Hence, the system remembers the initial configuration of the Fermi surface shrinks to a point, i.e. Fermi point. That is identified by a constant value of k_F and we arbitrary choose it to be equal to zero. In principle, we could shift the whole dispersion and k_F would be different. Such an initial configuration is reflected into the Green's function matrix element trend, as we discussed in Chapter 2. Indeed, its asymptotic trend shows exponentially decaying for large argument $R \gg \xi$, where ξ is the unique length scale in the system.
On the other side, the paper [16] has an initial Fermi Surface in its single-particle energy. This is an additional length degree of freedom, meaning we have a $\mathbf{k}_F$ 2D vector in the system. That presence adds a length scale which we are missing in our model, since we have only a Dirac point as 0-dimensional Fermi surface. Indeed, plotting the Green's function matrix elements of the paper, we find they possess an oscillatory trend. Probably, that oscillations are the source of high-values of Chern Numbers.
Our current guess is to introduce in the two-band model a non-zero chemical potential, i.e.

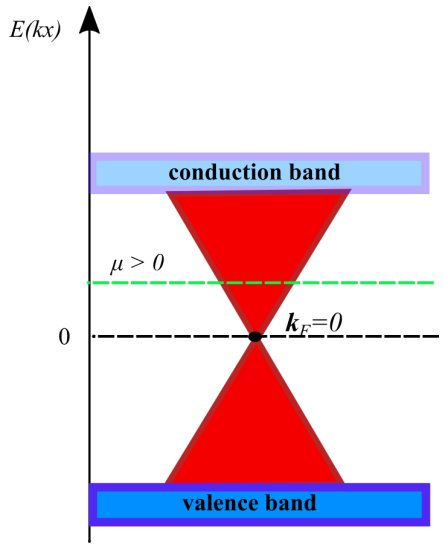

Figure 4.1: Sketch of an alternative model.

in the Hamiltonian a term like $\mu\mathbb{1}$ appears:

$$\hat{H} = \hat{H}_{\mathbf{k}}^{Surface} + |M|\tau_z + \hat{H}_{\mathbf{kk'}}^{Imp} + \mu\mathbb{1}.$$

We would like to see if the system responds like a Chern Insulator again or we might obtain some high-Chern numbers values. However, if these possible oscillations start after the cut-off of $5\xi/a$ we might not detect them in any case.
What matters, due to a $\mu \neq 0$, we introduce an additional length scale in the system and the Green's function matrix elements will definitely show a different trend - that worth investigating further.

Appendix A

Calculation of Bound State energy

Having as main reference the paragraph in Chapter 1 "Bound States from scattering process". Here, we present in more detail the calculation to find energy ω of bound states located at the impurity site.
The Hamiltonian of the scattering process in 1D regular lattice of spinless electrons over one static non-magnetic impurity - simply it is represented by a generic potential reads:

$$\hat{H} = \hat{H}_0 + \hat{V}.$$

The full propagator of the process, using the definition of T-matrix in eq.(1.7), in **r**-representation is given by:

$$\begin{aligned} &G^+(\mathbf{r},\mathbf{r}';\omega^+) = G_0^+(\mathbf{r}-\mathbf{r}';\omega) + G_0^+(\mathbf{r},0;\omega)T(0;\omega)G_0^+(0,-\mathbf{r}';\omega) \\ &\text{with } T(0;\omega) \equiv V\big(1 - G_0^+(0;\omega)V\big)^{-1}. \end{aligned}$$

The energy of bound states can be derived from the bound state condition, namely for those positive values ω that make vanishing the T-matrix:

$$T(0;\omega) = \frac{V}{1 - G_0^+(0;\omega)V} = 0 \Longleftrightarrow 1 - G_0^+(0;\omega)V = 0.$$

As initial step, we define the *spectral function* as:

$$\begin{aligned} \varrho(\omega) &= -\frac{1}{\pi}\Im\Big[G^+(\mathbf{r},\mathbf{r}';\omega^+)\Big] \\ &= -\frac{1}{\pi}\Im\Big[G_0^+(\mathbf{r}-\mathbf{r}';\omega) + G_0^+(\mathbf{r},0;\omega)T(0;\omega)G_0^+(0,-\mathbf{r}';\omega)\Big]. \end{aligned}$$

We know the object that encloses information at the impurity site is $G_0^+(0;\omega)$, hence we seek for an expression for it taking the imaginary part of $T(0;\omega)$.
Using the definition of Green's function given in eq.(1.5) and applying the Fourier Transform to **k**-representation we have:

$$\begin{aligned} \Im\Big[T(0;\omega)\Big] \Rightarrow \Im\Big[\lim_{\eta\to\,0^+} G_0^+(0;\omega+i\eta)\Big] &= \Im\int \frac{d\bar{\mathbf{k}}}{2\pi}\lim_{\eta\to\,0^+} G_0^+(0;\omega+i\eta)e^{i\bar{\mathbf{k}}\cdot 0} \\ &= \Im\int \frac{d\bar{\mathbf{k}}}{2\pi}\lim_{\eta\to\,0^+}\frac{1}{(\omega+i\eta)-\epsilon_{\bar{\mathbf{k}}}} \end{aligned}$$

where $\bar{\mathbf{k}}$ stands for the momentum of the particle freely moving among two following scattering processes and $\epsilon_{\bar{\mathbf{k}}} = \dfrac{\bar{\mathbf{k}}^2}{2m}$ is the one-particle energy dispersion.
If we want to relate the imaginary part of $G_0^+(0;\omega)$ with the spectral function $\varrho(\omega)$ we need to use the following identity:

$$\lim_{\eta\to\,0^+}\frac{1}{(\omega+i\eta)-\epsilon_{\bar{\mathbf{k}}}} = -i\pi\delta(\omega-\epsilon_{\bar{\mathbf{k}}}) + P\frac{1}{\omega-\epsilon_{\bar{\mathbf{k}}}}$$

where the first term is the result of the contour integration around the simple pole on the real axis (applying the *Residue-Cauchy Theorem*) and P represents the *Cauchy Principal Part* of the integral, an integration over real axis without simple poles on its path. Hence, filling in the identity:

$$\Im \int_{-\infty}^{\infty} \frac{d\bar{\mathbf{k}}}{2\pi} \left[-i\pi\delta\left(|\omega| - \frac{\bar{\mathbf{k}}^2}{2m}\right) + \mathrm{P}\, \frac{1}{\left(\omega - \dfrac{\bar{\mathbf{k}}^2}{2m}\right)} \right]. \tag{A.1}$$

To the current purpose, we employ only the first part of the such a limit. As evidence of that, the Principal Part will lead no contribution to the calculation. We would encounter integral of the type:

$$\int \frac{d\bar{\mathbf{k}}}{2\pi}\, \mathrm{P}\, \frac{1}{\left[\omega - \dfrac{\bar{\mathbf{k}}^2}{2m}\right]} = \int \frac{d\bar{\mathbf{k}}}{2\pi}\, \mathrm{P}\, \frac{-\sqrt{2m}}{\left[\bar{\mathbf{k}} - \sqrt{2m\omega}\right]\left[\bar{\mathbf{k}} + \sqrt{2m\omega}\right]}$$

If we evaluate the Principal Part for $\omega < 0$, the integral has imaginary poles, hence no physical energies can be extracted. In case of $\omega > 0$, we find two symmetric simple poles on the real axis. According to the usual contour of retarded propagator, the integral is convergent on the lower-complex plane. However, once we solve the integral by means of residue procedure, the two modified path running anticlockwise from the real axis to each poles have opposite sign. Hence, the residue is zero and neither this case gives contribution.
Going back to the main calculation we focused on the first part of (A.1). Using the δ-Dirac properties we obtain:

$$-\frac{1}{2}\int_{-\infty}^{\infty} d\bar{\mathbf{k}} \left[\delta\big(\sqrt{|\omega|} - \frac{\bar{\mathbf{k}}}{\sqrt{2m}}\big) \frac{1}{|\bar{\mathbf{k}}/m|} + \delta\big(\sqrt{|\omega|} + \frac{\bar{\mathbf{k}}}{\sqrt{2m}}\big) \frac{1}{|\bar{\mathbf{k}}/m|} \right].$$

Next, selecting the part that for $\omega > 0$ corresponds to real simple poles of $G_0^+(0;\omega)$:

$$-\frac{1}{2} 2\Theta(\omega) \int_0^{\infty} d\bar{\mathbf{k}}\delta\Big(\sqrt{\omega} - \frac{\bar{\mathbf{k}}}{\sqrt{2m}}\Big) \frac{1}{|\bar{\mathbf{k}}/m|} = -\sqrt{\frac{m}{2\omega}}.$$

Therefore, the derived expression of the imaginary part of the local bare propagator reads:

$$\Im\Big[\lim_{\eta \to\, 0^+} G_0^+(0;\omega + i\eta)\Big] = -\sqrt{\frac{m}{2\omega}}.$$

Finally, this result can directly be applied into the bound state condition, namely:

$$1 - G_0^+(0;\omega)V = 1 + \sqrt{\frac{m}{2\omega}}V = 0$$
$$\Rightarrow \omega = \frac{mV^2}{2}$$

and with this we have derived the energy of bound states located at the impurity site.

Appendix B

2D Fourier Transform Nearest-Neighbor Hopping model

The effective Hamiltonian in momentum space has an ideal form we can use to ultimately calculate the Chern Numbers of such system.
As an introductory study, see as further reference Shun [8], we consider a 2D square lattice of spinless electrons with a lattice constant. It is defined by the coordinates vectors:

$$\begin{aligned} &\mathbf{r}_i = \begin{pmatrix} ai \\ aj \end{pmatrix} \quad \mathbf{r}_j = \begin{pmatrix} ai' \\ aj' \end{pmatrix} \\ &|\mathbf{r}_{ij}| = a\sqrt{(i-i')^2 + (j-j')^2}. \end{aligned} \tag{B.1}$$

The energy spectrum of the collection of electrons will result into band structure - that process is embedded by Tight-Binding approximation.
We consider nearest-neighbor hopping (NN-hopping) - it is stated by the summation over $< i, j >$ - and we admit coupling between sites on x-axis and y-axis only.
Thus, the 2nd quantised Hamiltonian reads:

$$H_{ij} = -t \sum_{<i,j>} \left(c_{ij}^\dagger c_{i+1,j} + c_{i+1,j}^\dagger c_{ij} + c_{ij}^\dagger c_{i,j+1} + c_{i,j+1}^\dagger c_{ij} \right). \tag{B.2}$$

In momentum space we need to perform a 2D-Fourier Transform. Assuming periodic boundary conditions both in x and y directions - meaning both k_x, k_y are good quantum number to be used - that is defined by:

$$\begin{aligned} &k_x = \frac{2\pi}{aN_x} n, \quad n \in [0, N_x] \quad \text{and} \quad k_y = \frac{2\pi}{aN_y} n, \quad n \in [0, N_y] \\ &N_x \equiv N_y = N \\ &c_{ij}^\dagger = \frac{1}{N} \sum_{k_x, k_y} c_{k_x,k_y}^\dagger e^{-i(k_x(ai) + k_y(aj))} \end{aligned} \tag{B.3}$$

The resulting Hamiltonian is 0-dimensional in $\mathbf{k}$-space, since it written in terms of both k_x and k_y. We can split into cases for different or same impurity site as follow.
For any $i \neq j$, the Hamiltonian reads:

$$H_{ij} \Longrightarrow H_{k_x,k_y} = -2t \sum_{k_x,k_y} c_{k_x,k_y}^\dagger \big(\cos(ak_x) + \cos(ak_y) \big) c_{k_x,k_y} \tag{B.4}$$

For $i = j$, the Hamiltonian with no hopping process - thus we reduce to the case of one unique impurity in the lattice:

$$H_{ii'} = -t_0 \sum_{i,i'=1}^{N} c_{ii'}^\dagger c_{ii'} \Longrightarrow H_{k_x,k_y} = -t_0 \sum_{k_x,k_y} c_{k_x,k_y}^\dagger c_{k_x,k_y} \tag{B.5}$$

Therefore, the final Hamiltonian reads:

$$H_{k_x,k_y} = -\sum_{k_x,k_y} c^{\dagger}_{k_x,k_y}\Bigg(t_0 + 2\underbrace{t\Big(\cos(ak_x)+\cos(ak_y)\Big)}_{T}\Bigg)c_{k_x,k_y}. \tag{B.6}$$

If we introduce the 2D vector $\mathbf{k} = (k_x, k_y)$, the above Hamiltonian reads:

$$H_{\mathbf{k}} = -\sum_{\mathbf{k}} c^{\dagger}_{\mathbf{k}}\Big(t_0 + 2T\Big)c_{\mathbf{k}}. \tag{B.7}$$

Taking $\overrightarrow{C}_{\mathbf{k}}$ as a wave vector in $i = 1, .., N$, components, i.e.:

$$\overrightarrow{C}_{\mathbf{k}} = \begin{pmatrix} c_{\mathbf{k},1} \\ c_{\mathbf{k},2} \\ \vdots \\ c_{\mathbf{k},N} \end{pmatrix},$$

we can plug into the eigenvalue equation the derived Hamiltonian and we obtain:

$$E_{\mathbf{k}}\overrightarrow{C}_{\mathbf{k}} = H_{\mathbf{k}}\overrightarrow{C}_{\mathbf{k}}. \tag{B.8}$$

Thus, we can write down the explicit components:

$$E_{\mathbf{k}}\sum_{i=1}^{N} c_{\mathbf{k},i} = -\sum_{i=1}^{N}\Big(t_0 c_{\mathbf{k},i} + 2(T_{1,2}c_{\mathbf{k},i+1} + T^{\star}_{1,2}c^{\dagger}_{\mathbf{k},i-1})\Big) \tag{B.9}$$

that is

$$E_{\mathbf{k}}\begin{pmatrix} c_{\mathbf{k},1} \\ c_{\mathbf{k},2} \\ c_{\mathbf{k},3} \\ \vdots \\ c_{\mathbf{k},N} \end{pmatrix} = \begin{pmatrix} t_0 & 2T_{12} & 0 & \dots & \dots & \dots & 2T^{\star}_{12} \\ 2T^{\star}_{12} & t_0 & 2T_{12} & 0 & \dots & \dots & 0 \\ 0 & 2T^{\star}_{12} & T_0 & 2T_{12} & 0 & \dots & \vdots \\ \vdots & 0 & 2T^{\star}_{12} & t_0 & \dots & & \\ \vdots & \vdots & \vdots & \vdots & \ddots & \vdots & 2T_{12} \\ 2T_{12} & \dots & \dots & \dots & \dots & 2T^{\star}_{12} & t_0 \end{pmatrix} \cdot \begin{pmatrix} c_{\mathbf{k},1} \\ c_{\mathbf{k},2} \\ c_{\mathbf{k},3} \\ \vdots \\ c_{\mathbf{k},N} \end{pmatrix} \tag{B.10}$$

where we have

$$2T_{12} = 2t\Big(\cos(ak_x)+\cos(ak_y)\Big).$$

Thus, we recognise the pattern of an electron jumping one step along either $x-$ or $y-$ direction.
As a straightforward generalization, we can consider hopping process for long-range - still coupling only on $x-$ and $y-$ direction. The Hamiltonian in components reads:

$$E_{\mathbf{k}}\sum_{i=1}^{N} c_{\mathbf{k},i} = -\sum_{i=1}^{N}\Big(t_0 c_{\mathbf{k},i} + 2(T_{1,i+1}c_{\mathbf{k},i+1} + T^{\star}_{1,i-1}c^{\dagger}_{\mathbf{k},i-1})\Big) \tag{B.11}$$

hence

$$2T_{12} = 2t\Big(\cos(ak_x)+\cos(ak_y)\Big)$$
$$2T_{13} = 2t\Big(\cos(2ak_x)+\cos(2ak_y)\Big)$$
$$2T_{14} = 2t\Big(\cos(3ak_x)+\cos(3ak_y)\Big)$$

where we identify each term as NN-hopping, the Next-NN-hopping and so on.
In Chapter 3 we will perform a full Fourier Transform over all lattice sites in any direction, not only on the main axes than.

Appendix C

Calculation of $G_0^+(|r-r'|)$ in 2D with Bessel Functions

The present appendix presents the derivation of the local bare propagator for a lattice of impurity. More details can be found in Gradshteyn [18] and Abramowitz [19].

The Bessel functions notation: K(z) is Second Kind Modified Bessel function, J(z) First Kind Bessel function.
We make use of the following integral formulas:

$$\int_0^{2\pi} d\theta e^{i(a\cos\theta+n\theta)} = 2\pi i^n J_n(a) \tag{C.1}$$

with $a \in \mathbb{R}^+$;

$$\int_0^{+\infty} dx \frac{x}{x^2+k^2} J_0(ax) = K_0(ax) \tag{C.2}$$

with $a > 0$, $\Re[k] > 0$.
The derivative of the Bessel function with respect of its argument:

$$\frac{\partial}{\partial x} J_0(x) = -J_1(x) \quad , \quad \frac{\partial}{\partial x} K_0(x) = -K_1(x) \tag{C.3}$$

The identity:

$$J_{-n}(x) = (-1)^n J_n(x) \tag{C.4}$$

for $n \in \mathbb{Z}$.

Retarded propagator in 2D

We want to derive an expression for the Green's function:

$$\mathcal{G}_0^+(\mathbf{r}=\mathbf{r}_j-\mathbf{r}_i;E) = \begin{pmatrix} X_0(|\mathbf{r}|)+X_1(|\mathbf{r}|) & X_2^+(|\mathbf{r}|) \\ X_2^-(|\mathbf{r}|) & X_0(|\mathbf{r}|)-X_1(|\mathbf{r}|) \end{pmatrix}$$

with matrix elements - recalling $\mathcal{G}_0^+(\mathbf{k};E)$ in eq.(2.22)

$$X_0(\mathbf{r})\mathbb{1} = (E\mathbb{1}) \int_0^\Lambda \frac{d^2\mathbf{k}}{(2\pi)^2} \frac{e^{-i\mathbf{k}\cdot\mathbf{r}}}{E^2-M^2-v_F^2|\mathbf{k}|^2}$$

$$X_1(\mathbf{r})\tau_3 = (M\tau_3) \int_0^\Lambda \frac{d^2\mathbf{k}}{(2\pi)^2} \frac{e^{-i\mathbf{k}\cdot\mathbf{r}}}{E^2-M^2-v_F^2|\mathbf{k}|^2}$$

$$X_2^\pm(\mathbf{r})(\tau_1+\tau_2) = \int_0^\Lambda \frac{d^2\mathbf{k}}{(2\pi)^2} \frac{k_x \pm ik_y}{E^2-M^2-v_F^2|\mathbf{k}|^2} e^{-i\mathbf{k}\cdot\mathbf{r}}.$$

The resolution for X_0, X_1 starts with writing the integral in polar coordinates, then:

$$\begin{aligned}
X_{0,1}(\mathbf{r}) &= (E\mathbb{1} + M\tau_3)\int_0^{+\infty}\frac{dk}{(2\pi)^2}\frac{-k}{\frac{M^2-E^2}{v_F^2}+k^2}\int_0^{2\pi}d\theta_k e^{ik\cdot r\cos(\theta_k-\theta_r)} \\
&= (E\mathbb{1} + M\tau_3)\int_0^{+\infty}\frac{dk}{(2\pi)}\frac{-k}{\frac{M^2-E^2}{v_F^2}+k^2}J_0(kr) && \text{using C.1 for } kr\in\mathbb{R}^+ \\
&= -\frac{(E\mathbb{1} + M\tau_3)}{2\pi}K_0\Big(|r|\frac{\sqrt{M^2-E^2}}{v_F}\Big) && \text{using C.2 for } \Re(M)>\Re(E)
\end{aligned}$$

The resolution for $X_2^{\pm}$ starts similarly. In addition, we introduce the following notation:
$v_F(k_x \pm ik_y) = v_F k(\cos\theta \pm i\sin\theta) = v_F k \times e^{\pm i\theta_k}$
$v_F(r_x \pm ir_y) = v_F r(\cos\theta \pm i\sin\theta) = v_F r \times e^{\pm i\theta_r}$
that is because the scalar product between $k\cdot r$ is generically taken for non-aligned r component to the x-axis. Hence, we calculate for the X_2^+:

$$\begin{aligned}
X_2^+(\mathbf{r}) &= -\frac{1}{(2\pi)^2}\int_0^{+\infty}dk\frac{k}{\frac{M^2-E^2}{v_F^2}+k^2}\int_0^{2\pi}d\theta_k k e^{i\theta_k}e^{-i(k\cdot r\cos(\theta_k-\theta_r))} \\
&= \frac{-ie^{i\theta_k}}{2\pi}\int_0^{+\infty}dk\frac{k}{\frac{M^2-E^2}{v_F^2}+k^2}(-k)J_1(kr) && \text{using C.1 for } kr\in\mathbb{R}^+ \\
&= \frac{-i}{2\pi}\frac{\partial}{\partial_r}\int_0^{+\infty}dk\frac{k}{\frac{M^2-E^2}{v_F^2}+k^2}J_0(kr) && \text{using C.3} \\
&= \frac{-iv_F}{2\pi}\frac{\partial}{\partial_r}K_0\Big(|r|\frac{\sqrt{M^2-E^2}}{v_F}\Big) && \text{using C.2 for } \Re(M)>\Re(E) \\
&= \frac{-iv_F}{2\pi}\frac{\sqrt{M^2-E^2}}{v_F}K_1\Big(|r|\frac{\sqrt{M^2-E^2}}{v_F}\Big) && \text{using C.3}
\end{aligned}$$

Similar for $X_2^-(\mathbf{r})$, just with opposite sign.
Using the derived correlation length $\xi = \dfrac{v_F}{\sqrt{M^2-E^2}}$, the final version reads:

$$\begin{aligned}
\mathcal{G}_0^+(\mathbf{r}=\mathbf{r}_j-\mathbf{r}_i;E) &= -\frac{1}{2\pi}\begin{pmatrix} E+M & iv_F e^{i\theta_r}\partial_{|r|} \\ -iv_F e^{-i\theta_r}\partial_{|r|} & E-M\end{pmatrix}K_0\Big(\frac{|\mathbf{r}|}{\xi}\Big) \\
&= -\frac{1}{2\pi}\begin{pmatrix} (E+M)K_0\Big(\frac{|\mathbf{r}|}{\xi}\Big) & -i\frac{v_F}{\xi}e^{i\theta_r}K_1\Big(\frac{|\mathbf{r}|}{\xi}\Big) \\ -i\frac{v_F}{\xi}e^{-i\theta_r}K_1\Big(\frac{|\mathbf{r}|}{\xi}\Big) & (E-M)K_0\Big(\frac{|\mathbf{r}|}{\xi}\Big)\end{pmatrix}
\end{aligned} \tag{C.5}$$

Asymptotic behaviour

The Second Kind Modified Bessel function K(z) has the following asymptotic expansion series.
For $z \longrightarrow 0$:

$$\begin{aligned}
K_0(z) &\propto -\log\frac{z}{2}\Big(1+\mathcal{O}(z^2)\Big) \\
K_1(z) &\propto \frac{1}{z}\Big(1+\mathcal{O}(z^2)\Big) + \frac{z}{2}\log\frac{z}{2}\Big(1+\mathcal{O}(z^2)\Big)
\end{aligned}$$

and in particular $K_0(0) = \infty$.
Thus, using such expansion, for $|r| \longrightarrow 0$ i.e. in terms of correlation length scale $|r| \ll \xi$, the Green's function $\mathcal{G}_0^+(r; E)$ reads:

$$\mathcal{G}_0^+(r; E^+) \sim \frac{-1}{2\pi} \begin{pmatrix} E+M & iv_F e^{i\theta_r}\partial_{|r|} \\ -iv_F e^{-i\theta_r}\partial_{|r|} & E-M \end{pmatrix} \log\left(\frac{|r|}{2\xi}\right).$$

For $z \longrightarrow \infty$ and $\nu \in \mathbb{Z}$:

$$K_\nu \propto \sqrt{\frac{\pi}{2}}\frac{e^{-z}}{\sqrt{z}}\Big(1 + \mathcal{O}(\frac{1}{z})\Big)$$

and in particular $\lim_{z\to\infty} K_\nu(z) = 0$.
Thus, using such expansion, for $|r| \longrightarrow \infty$ i.e. in terms of correlation length scale $|r| \gg \xi$, the Green's function $\mathcal{G}_0^+(r; E)$ reads:

$$\mathcal{G}_0^+(r; E) \sim -\frac{1}{2\sqrt{2\pi}} \begin{pmatrix} E+M & iv_F e^{i\theta_r}\partial_{|r|} \\ -iv_F e^{-i\theta_r}\partial_{|r|} & E-M \end{pmatrix} \frac{e^{|r|/\xi}}{\sqrt{|r|/\xi}}.$$

These trends have a relevant interpretation in the model, namely they count whether or not coupling among impurities is for short or long distance with respect to the correlation length - see Chapter 2.

Bibliography

[1] A. Altland and B. Simons, *Condensed Matter Field Theory*, Cambridge University Press, 2010.

[2] H. Bruus, K. Flensberg, *Many-Body Quantum Theory in Condensed Matter*, 2nd Edition, Oxford University Press, 2002.

[3] Micheal A. Parker, *Solid State and Quantum Theory for optoelectronics*, CRC Press, 2010.

[4] Manfred Sigrist, *lecture notes Solid State Physics* 2014.

[5] Eleftherios N. Economou, *Green's functions in Quantum Physics*, 3rd Edition, Springer, 2005.

[6] Gerald D. Mahan, *Many-Particle Physics*, 3rd Edition, Kluwer Academic/Plenum Publishers, 2000.

[7] G. Tkachov, *Topological Insulators*, Pan Stanford Publishing, 2016.

[8] Shun-Qing Shen, *Topological Insulators - Dirac Equation in Condensed Matters*, Springer Series in Solid-State Sciences, 2012.

[9] J. K. Asbóth, L. Oroszlány, A. Pályi, *A short course on Topological Insulators*, https://arxiv.org/pdf/1509.02295.pdf.

[10] B. Andrei Bernevig with Taylor L. Hughes, *Topological Insulators and Topological Superconductors*, Princeton University Press, 2013.

[11] F.D.M. Haldane, *Model for a Quantum Hall Effect without Landua Levels: Condensed-Matter realization of the "Parity Anomaly"*, Phys. Rev. Lett. 61, 2015 - published 31st October 1988, https://doi.org/10.1103/PhysRevLett.61.2015.

[12] M.Z. Hasan, C.L. Kane, *Colloquium: Topological Insulators*, Rev. Mod. Phys. 82, 3045, https://doi.org/10.1103/RevModPhys.82.3045.

[13] TU Delf online course, *Topology in Condensed Matter*, https://topocondmat.org/.

[14] M. Franz, L. Molenkamp, *Contemporary Concepts of Condensed Matter Science: Topological Insulator*, Elsevier, 2013.

[15] Chao-Xing Liu, Shou-Cheng Zhang, Xiao-Liang Qi, *The quantum anomalous Hall Effect*, https://arxiv.org/pdf/1508.07106.pdf.

[16] V. Kaladzhyan, J. Röntynen, P. Simon, T. Ojanen, *Topological state engineering by potential impurities on chiral superconductors*, Phys. Rev. B 94, 060505(R), https://doi.org/10.1103/PhysRevB.94.060505.

[17] R-J Slager, L. Rademaker, J. Zaanen, and L. Balents, *Impurity-bound states and Green's function zeros as local signatures of topology*, Phys. Rev. B 92, 085126, https://doi.org/10.1103/PhysRevB.92.085126.

[18] I. S. Gradshteyn, I. M. Ryzhik, *Table of Integrals, Series and Products*, 4th Edition, Academic Press, Inc., 1980.

[19] M. Abramowitz, I. A. Stegun, *Handbook of Mathematical Functions with formulas, graphs, mathematical tables*, 10th printing, National Bureau of Standards Applied Mathematics Series 55, 1972.